

Research Paper

Global sensitivity analysis of a generator-absorber heat exchange (GAX) system's thermal performance with a hybrid energy source: An approach using artificial intelligence models



V. Cardoso-Fernández^a, A. Bassam^b, O. May Tzuc^{c,*}, M.A. Barrera Ch.^d, Jorge de Jesús Chan-González^c, M.A. Escalante Soberanis^b, N. Velázquez-Limón^e, Luis J. Ricalde^{b,*}

^a Posgrado en Ingeniería, Facultad de Ingeniería, Universidad Autónoma de Yucatán, Av. Industrias No Contaminantes por Anillo Periférico Norte, Apdo. Postal 150, Cordemex, Mérida, Yucatán, Mexico

^b Facultad de Ingeniería, Universidad Autónoma de Yucatán, Av. Industrias No Contaminantes por Anillo Periférico Norte, Apdo. Postal 150, Cordemex, Mérida, Yucatán, Mexico

^c Facultad de Ingeniería, Universidad Autónoma de Campeche, Campus V, S/N por Av. Humberto Lanz Cárdenas y Unidad Habitacional Ecológica Ambiental, Col. Ex Hacienda Kalá, C.P. 24085, San Francisco de Campeche, Campeche, Mexico

^d H&H Construcción, Nogal #111 col. El Tezontle, Pachuca de Soto Hidalgo 42084, Mexico

^e Centro de Estudios de las Energías Renovables (CEENER), Instituto de Ingeniería, Universidad Autónoma de Baja California, Calle de la Normal S/N, Mexicali, Baja CA, Mexico

ARTICLE INFO

ABSTRACT

Keywords:

Generator-Absorber Heat Exchange (GAX)
Solar refrigeration cycle
Hybrid renewable energy system
Data-driven models
PAWN method
Decision-making process
Absorption refrigeration

Generator-absorber heat exchange (GAX) systems represent a promising alternative to substitute environmentally harmful refrigeration devices based on conventional vapor compression, as long as a proper analysis of thermal performance and the complex interactions of heat transfer that occur into GAX cycle is taken in consideration. In this research, a cooling process based on a GAX system that uses ammonia-water working fluid and a hybrid source (natural gas-solar) is studied to analyze the variables that affect the system's thermal performance. The work's novelty is the hybridization between artificial intelligence (AI) modeling and the global sensitivity analysis (GSA) developed with the PAWN method. Experimental data was obtained from a system with a cooling capacity of 10.5 kW (3 Ton), designed to work at heat source temperatures of 200 °C. The measured variables were the temperatures at generator, heat at evaporator, and working fluid volumetric flow. Three AI techniques (artificial neural networks, genetic programming, and support vector machines) were evaluated for modeling the thermodynamic cycle. Results obtained from the PAWN method applied to the artificial neural network, since it was the best AI model, indicates that the operational parameters with a greater impact in the system's performance are the inlet temperature at the generator (30.7 %) and the heat measured at the evaporator for NH₃ (27.4 %), for the first output COP_{NH₃}. For the second output COP_{H₂O}, the inlet temperature at the generator (32.5 %) and the heat measured at the evaporator for H₂O (26.7 %), have a greater impact for such output. The proposed IA-GSA methodology contributes to the development of operational decision-making related to instrumentation, operation performance, and corrective and/or preventive maintenance actions of GAX systems. The developed thermal performance model has potential for implementation in embedded systems (smart sensors) as a critical element in control and optimization strategies to improve the performance of these cycles.

1. Introduction

Humanity is at a stage where the need to find ways to reduce the

emission of polluting gases is growing day by day, mainly in processes associated with the commercial [1,2] and industrial [3,4] sectors. As each country is responsible for its own emissions, each commercial and industrial sector is linked to a certain amount of polluting gases. It is

* Corresponding authors.

E-mail addresses: oscajmay@uacam.mx (O. May Tzuc), lricalde@correo.uday.mx (L.J. Ricalde).

Nomenclature	
α_i, α_i^*	Lagrange multipliers of the SVM model
b_{ANN}	Bias assigned to the neurons of the ANN model
b_{GP}	Bias of the GP model
b_{SVM}	Bias parameter of the SVM model
C	Regularization constant of the SVM model
C_{sp}	Specific heat of the thermal oil [J/kg °C]
c_m	Weight of the elements in the kernel layer of the SVM model
COP_{H2O}	Coefficient of performance for H_2O [-]
COP_{NH3}	Coefficient of performance for NH_3 [-]
ΔT_{oil}	Difference of temperature between the inlet and outlet of the generator [°C]
ϵ	Loss function of the SVM model
F_{oil}	Mass flow of the thermal oil [kg/s]
F_y	Volumetric flow of the working fluid [L/min]
$F_y(y)$	Unconditional CDF
$F_{y,xi}(y)$	Set of conditionals CDF
f	Transfer functions of the ANN model
G_i	Genes of the GP model
h_n	Weight associated with each gene of the GP model
H_2O_{flow}	Mass flow for cold water generation [kg/s]
H_2O_{in}	Input evaporator temperature for cold water generation [°C]
H_2O_{out}	Output evaporator temperature for cold water generation [°C]
$K(x)$	Space with higher-dimension properties of the SVM model
$K\langle x_i, x \rangle$	Kernel function of the SVM model
\dot{m}_{ab}	Mass flow of the cooling air at the absorber [m^3/s]
\dot{m}_{co}	Mass flow of the cooling air at the condenser [m^3/s]
\dot{m}_{heat}	Mass flow of the heating oil [kg/s]
\dot{m}_{re}	Mass flow of the cooling air at the rectifier [m^3/s]
\dot{m}_{ref}	Mass flow of the refrigerant [kg/s]
\dot{m}_{ss}	Mass flow of the strong solution [kg/s]
\dot{m}_{ws}	Mass flow of the weak solution [kg/s]
NN	Number of model evaluations for the GSA
NH_{3ref}	Ammonia concentration of the refrigerant [%]
NH_{3ss}	Ammonia concentration of the strong solution [%]
NH_{3ws}	Ammonia concentration of the weak solution [%]
N_c	Random samples generated for the conditional set of the GSA
N_u	Random samples generated for the unconditional set of the GSA
n_{ANN}	Sum of the weights and bias assigned to the input neurons of the ANN model
n_{DB}	Number of elements in the database
n_{GP}	Genes considered by the GP model
n_{SA}	Random samples created for the GSA
n_{SVM}	Number of support vectors of the SVM model
P	Number of input variables of the ANN model
P_{ab}	Pressure at the absorber [MPa]
P_{co}	Pressure at the condenser [MPa]
P_{ev}	Pressure at the evaporator [MPa]
P_{ge}	Pressure at the generator [MPa]
p	Number of neurons in the input layer of the ANN model
$Q_{ev,H2O}$	Heat at the evaporator measured for H_2O [kW]
$Q_{ev,NH3}$	Heat at the evaporator measured for NH_3 [kW]
Q_{gen}	Heat measured at the generator [kW]
R	Number of neurons in the hidden layer of the ANN model
σ, ε	Cost misclassification numbers of the SVM model
$(\vartheta_i, \vartheta_i^*)$	Slack variables of the SVM model
$T_{g,in}$	Temperature at the inlet of the generator [°C]
$T_{g,out}$	Temperature at the outlet of the generator [°C]
T_{mn}	Sensitivity index [-]
W	Work done by the system's components [kW]
w	Weight assigned to the neurons of the ANN model
w^T	Weight vector of the SVM model
x_{ANN}	Input neurons of the ANN model
x_{SVM}	Input's space of the SVM model
$\bar{X}_{n,n}$	Input parameters fixed for the GSA
y	Set of experimental values for a specific variable
Y_{ANN}	Output generated by the ANN model
$Y_{exp(i)}$	Experimental output used for the statistical evaluation
Y_{GP}	Output generated by the GP model
Y_{max}	Maximum value of the y set
Y_{min}	Minimum value of the y set
Y_N	Normalized set of values
$Y_{sim(i)}$	Simulated output used for the statistical evaluation
Y_{SVM}	Output generated by the SVM model
Abbreviations	
AHX	Absorber heat exchanger
AI	Artificial intelligence
ANN	Artificial neural network
BR	Bayesian Regulation
CDF	Cumulative distribution function
COP	Coefficient of performance
EES	Engineering Equation Solver
GAX	Generator-absorber heat exchange
GP	Genetic Programming
GSA	Global Sensitivity Analysis
HCFCs	Hydrochlorofluorocarbons
HVAC	Heating, ventilation and air conditioning
KS	Kolgomorov-Smirnov static
LM	Levenberg-Marquardt
MAE	Mean absolute error
MSE	Mean square error
RMSE	Root mean square error
RTD	Resistant Temperature Detection
SA	Sensitivity analysis
SCG	Scaling Conjugate Gradient Backpropagation
SNR	Substitution Newton-Raphson method
SVM	Support Vector Machine
VCRS	Mechanical vapor compression system

estimated that worldwide, 15 % of the energy consumed is destined for the cooling of spaces at different scales [5]. In this context, refrigeration systems based on mechanical vapor compression (VCRS) currently represent one fifth of the energy consumed internationally. One of the main consequences of this percentage of energy consumption is the generation of large amounts of hydrochlorofluorocarbons (HCFCs), which deteriorate the ozone layer and contribute 10 % to the increase in global temperature [6,7].

Since absorption systems consume less energy than VCRS systems and are capable of working with refrigerants that emit a lower amount of polluting gases into the atmosphere, they are considered as an attractive alternative to reduce the environmental impact associated with cooling systems. Additionally, different types of technologies based on renewable energies can be coupled to absorption systems, providing part of the energy demanded by the generator and thus contributing to the decarbonization of refrigeration systems [8–10].

Within the options of absorption refrigeration systems, generator-absorber heat exchange (GAX) cycles are considered one of the most prominent options currently on the market, due to their low cost and complexity, compared to other technologies such as single and multiple-effect absorption cycles [11]. The implementation of technologies that uses renewable energy sources on GAX cycles have made it possible to improve the coefficient of performance (COP) of the hybrid system compared to the traditional cycle [12], consequently reducing the amount of polluting particles emitted into the environment [13].

The main characteristic of the GAX system is the temperature difference presented between the absorber and the generator, which is achieved by a concentration gradient between the weak and a strong solution. The idea consists of obtaining high temperatures in the operational sections of the absorber. This eventually leads to a reduction of the external heat needed by the generator and improve the system's efficiency, measured by the coefficient of performance (COP).

Different variations have been made on the GAX cycle in order to improve the system's COP. For the simple GAX cycle, studied in this work, the absorber and generator are maintained at pressure and temperature conditions such that a temperature difference is created, which is directed to the generator, increasing the COP. In [14,15], the competitive operating conditions associated with a hybrid GAX heat pump system were obtained, highlighting the low ambient temperature (7°C), abundant solar radiation (800W/m^2) and operating temperature (180°C).

In [16], a two-stage GAX cycle with an absorption-reabsorption heat pump is developed employing an internal heat recovery system for sites where the ambient temperature is low for most time of the year. The results show that the maximum COP reached is 1,367, supplying heat at a temperature of 46.1°C ; both quantities obtained at ambient temperatures above -15.6°C . In most cases, heat was obtained with a temperature above 42°C , ideal for heating buildings.

In addition to the experimental systems previously exposed, different computational studies have been developed to model and optimize the performance of hybrid GAX systems [17,18]. In [17], as a modeling alternative for the complex thermodynamic performance equations, a surrogate model using artificial neural networks (ANN) is implemented, in order to obtain a relationship for the COP and the circulation ratio (f) as a function of the temperatures of the generator, evaporator, condenser and absorber, as well as the concentration of the weak and strong solutions. Using the mean squared error statistical coefficient (R^2) as an evaluation instrument for the ANN model, values of 0.9873 and 0.9996 are obtained for the COP and f , respectively, indicating a high reliability relationship of the model.

In [18] is presented a technical and financial evaluation of a cooling system with solar absorption. The impact that the size of the absorption subsystem and volume of the storage tank have on the cycle is analyzed with global optimization using genetic algorithms. The results indicate that the optimal configuration for the hybrid system consists of an absorption subsystem with a capacity of $0.04\text{--}0.06\text{ kW/m}^2$ and a storage tank with a volume of $40\text{--}60\text{ L/m}^2$. This optimized system has a payback period of 4.96 years and allows for annual energy savings of up to 68.8 kWh/m^2 .

Due to the fact that thermal refrigeration processes can present complex relationships between the study variables, the use of advanced computing techniques is often required to represent them. In this context, artificial intelligence models have been used to solve problems associated with different thermal systems, such as the exergetic analysis of VCRS [19], the study of operational parameters such as the operating temperature and the working fluid [20] and prediction of heating, ventilation and air conditioning (HVAC) performance [21], among others. According to a trend analysis, one of the main characteristics studied in refrigeration systems through artificial intelligence techniques is the COP [7].

Artificial intelligence models are suitable for studying the multiple

stages that make up the GAX cycle, modeling the interaction between operational variables and system performance. In addition, the interest of carrying out the global sensitivity analysis lies in the possibility of determining the importance associated with each independent variable in relation to the output parameters studied. The use of these models is justified considering the complexity of the absorption, generation, evaporation and condensation sections that make up the GAX cycle as well as any other refrigeration system, where multiple independent variables are measured in order to determine their association through a data-driven model [7].

As a summary, Table 1 shows the articles analyzed in this section with their most relevant characteristics, in which experimental or computational studies on GAX cycles are developed. The choice of these articles is based on the relevance that it has for the present work the obtaining of output variables for the GAX cycle, either experimentally or computationally, as well as the operational parameters measured in the different refrigeration systems. As can be seen in Table 1, most of the recent investigations of the GAX cycle presents a computational approach. Within the objectives set by each author, it is observed that the evaluation of the operational parameters and how they affect the system's performance are the most prominent studies. Also, the combination of $\text{NH}_3/\text{H}_2\text{O}$ has been one of the most studied working fluids for the GAX cycles.

However, some limitations have been found in the previous research reported in Table 1. In the experimental type of studies, they only establish correlations between a few operating parameters, such as the driving temperature, low-grade heat source temperature, supply water temperature, with outputs like the system's performance and solar fraction [14,22]. As for the computational studies, they mostly use methodologies created to optimize or improve certain performance parameters, without considering a previous analysis of variables, which can help to reduce the complexity of the studied problem [15,23]. Sensitivity analysis applied to a data-based refrigeration model is a major gap of knowledge found in the literature review. This hybrid methodology can help to improve any optimization processes, by choosing only the variables with a higher relative influence regarding the studied output.

In the literature review, no works have been found that use Artificial Intelligence models (AI) to perform the computational representation of a GAX cycle, to later carry out a Global Sensitivity Analysis (GSA) of the operational parameters of the system. In this context, the novelty of this work consists in:

- Creating a hybrid computational methodology, based on artificial intelligence techniques, capable of being applied to GAX systems.
- Contributing to a better understanding of the coefficient of performance (COP) of a GAX system.
- Integrating the AI models to a Global Sensitivity Analysis (GSA) through the PAWN method, with the objective of determine which are the operational variables of a GAX cycle that have a greater impact on the coefficient of performance (COP).

By considering such methodology, the results of this work are intended to be an auxiliary criterion for decision making, seeking to establish the main operational parameters that must be modified, in order to achieve an increase in the efficiency of the refrigeration system.

The manuscript is organized as follows: Section 2 describes the experimental system, the design parameters and the different stages that the working fluid goes through in the cycle. Section 3 presents the methodology to be followed, divided into three subsections: Processing and analysis of the experimental database, creation of artificial intelligence models and global sensitivity analysis using the PAWN method. Section 4 is integrated by the discussion of the results, dedicating a subsection for each stage of the methodology. Finally, Section 5 presents the conclusions of the study.

Table 1

Statement of the problem for studies that use refrigeration systems based on the GAX cycle.

Reference	Objective	Type of study	Working fluid	AI + GSA
Dai et al. [14]	Increase the percentage of solar energy used in the GAX cycle	Experimental	NH ₃ /H ₂ O	No
Braga & Figueiredo [23]	Develop a methodology that allows simulating and optimizing operational parameters of the GAX cycle	Computational Modeling technique: Substitution Newton-Raphson method (SNR) [24]	NH ₃ /H ₂ O	No
Wang et al. [22]	Evaluate the performance of the GAX cycle under different operational conditions	Experimental	NH ₃ /H ₂ O	No
Mohammadi et al. [25]	Improve efficiency and reduce capital and operating costs, as well as the levelized costs of hybrid GAX cycles	Economic-environmental Modeling technique: Steady-state simulation with Engineering Equation Solver (EES)	CO ₂ /NH ₃	No
Liu et al. [26]	Promote the application of ACHP systems by obtaining optimal operating conditions and creating a new performance coefficient	Computational Modeling technique: Steady-state simulation with Engineering Equation Solver (EES)	NH ₃ /H ₂ O	No
Wu y Leung [27]	Optimize the refrigerant injection rate in a HEHP cycle to maximize overall primary energy efficiency	Computational Modeling technique: Steady-state simulation with Engineering Equation Solver (EES)	NH ₃ /LiNO ₃	No
Xu et al. [18]	Describe a viable solution for cooling systems with thermal storage through solar energy	Computational Modeling technique: Matlab environment, using REFPROP 9 and ICE-E.	LiBr/H ₂ O	No
Dai et al. [15]	Determine the optimal operating conditions of a GAX cycle with solar energy and natural gas as heat source	Computational Modeling technique: Steady-state simulation with Engineering Equation Solver (EES)	NH ₃ /H ₂ O	No
Mahmoudi et al. [28]	Optimization of a heat transformer and refrigeration system integrated with a water desalination system	Experimental-Computational Modeling technique: Thermoeconomic modeling of governing equations	LiBr/H ₂ O	No
This work	Determine the influence of operating parameters on the GAX performance, by using a hybrid computational methodology	Experimental-Computational Modeling technique: Artificial Intelligence models (AI) coupled with PAWN method for Global Sensitivity Analysis (GSA)	NH ₃ /H ₂ O	Yes

2. System description

The experimental facility to obtain the 10.5 kW GAX system's performance data is described in Fig. 1. It is integrated by a generator, condenser, evaporator, and absorber that operates with pair ammonia-water (NH₃–H₂O) mixture as working fluid; with the elements designed to be air-cooled. The generator and the absorber are divided into smaller sections in order to increase the amount of heat received by the working fluid and therefore reducing the external heat demanded (generator) and the cooling requirements (absorber). The system is complemented by a pre-cooling device for the working fluid added between the condenser and evaporator, and a rectifier integrated into the generator needed to purify the refrigerant before entering the condenser. Additionally, the GAX system is equipped with two expansion valves and a solution pump for the working fluid.

Fig. 2 illustrates the schematic diagram of the GAX system's operation. The ammonia vapor (99 % pure) leaves the rectifier towards the condenser as a high-pressure saturated vapor. Inside the condenser, this is converted into a saturated liquid and sent to the pre-cooling element to reduce its temperature. Subsequently, the fluid is circulated through the pressure valve (V1) to obtain a liquid-vapor mixture at low pressure. In the evaporator, this mixture receives the heat from the water intended to be cooled, generating the refrigeration effect for the demanded application. Once its cooling function has been fulfilled, the mixture is recirculated through the pre-cooler (heat exchanger) to take advantage of the heat from the counter flow pipe and evaporate the remaining liquid. This cooled vapor enters at the absorber's bottom, where it is absorbed by a NH₃/H₂O poor ammoniacal solution. From this point on, exothermic phase changes are generated, requiring heat exchangers in the lower element of the absorber. This aqueous solution now with a high percentage of refrigerant (also called strong solution) is pumped at high pressure toward the next absorber element (AHX), where it receives heat from the absorber. By entering the third and hottest element (GAX), it receives even more heat from the absorber, reaching its saturation point and leaving the absorber again as a liquid-vapor mixture. This mixture enters a chamber between the generator and the rectifier. In this stage, the liquid phase of the liquid-vapor mixture coming from the absorber gets in contact with the condensed vapor coming from the rectifier and they both enter the generator, where the refrigerant is extracted from the solution. This weak solution, with a low percentage of refrigerant, exits through the bottom of the section. The solution is heated in the generator by external sources and enters again the generator to deliver this heat in the GHX section. The second pressure valve (V2) returns it to low pressure, making it able to return to the absorber at its higher section, where it encounters the vapor refrigerant. Back in the generator, the released refrigerant vapor goes through three sections, two external heat sources and a GHX. Afterwards, it enters the heat exchange chamber, with the vapor coming from the absorber. This vapor ascending flow enters the rectifier, where the heavier element (water) condenses. This leads to a highly pure refrigerant, ready to restart the cycle [12,29]. For the replication of the present work, the characteristics mentioned in Table 2 must be considered.

It is important to emphasize that the system has the capacity to work with natural gas and solar energy as external energy sources. The working fluid at the generator is heated up to 287 °C using a Chromalox device. By varying the temperature of this instrument, it is possible to represent different configurations of the solar thermal technology in order to create a robust database for a deeper numerical analysis and proper control of the experimental system.

Facility was instrumented with a series of sensors in order to measure the thermodynamic properties of interest (Fig. 2). Resistant Temperature Detection sensors (RTD) were used to obtain the inlet and outlet temperature of the generator. RTDs present a temperature range of -180 °C to 480 °C, and were calibrated by using the electronic caliper AMETEK Jofra Inst., model D55SE. Measurement of volumetric flow were conducted by Ft4-8NEXW-LEG-5 electromagnetic turbine flow

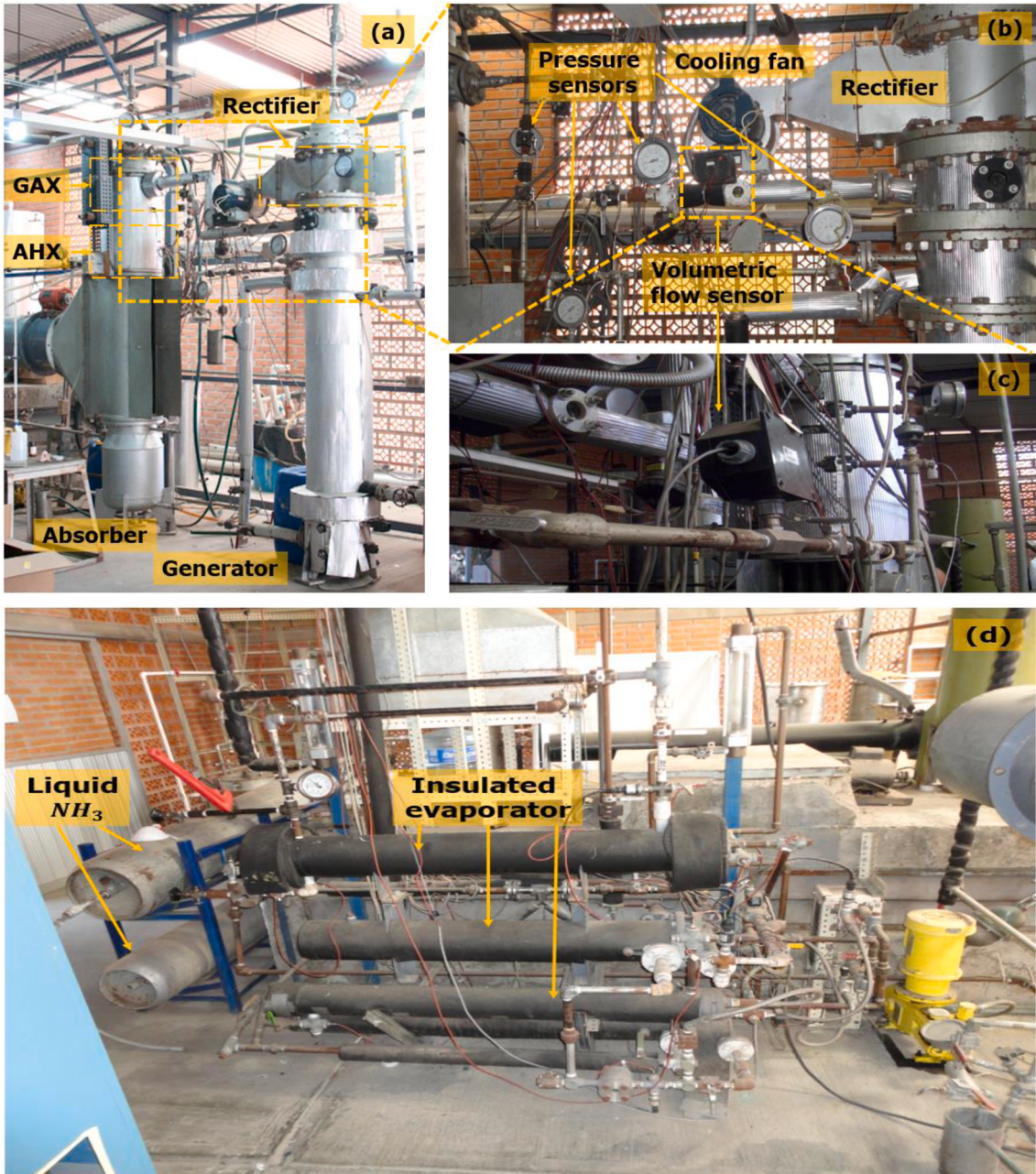


Fig. 1. Setup of the experimental GAX system: (a) Absorber column with the GAX and AHX sections (left) along with the generator and rectifier (right); (b) Close up of the absorber-generator connection with their corresponding pressure and volumetric sensors; (c) Volumetric sensor profile view; (d) Refrigerant tanks connected to the evaporator.

sensors from Flow Technology Inc. Finally, pressure was measured by transducer type EA, belonging to Data Instrument Corporation. The data acquisition system Hewlett Packard model HP 3852A, was used to collect the measurements made by each instrument. It consists of three multiplexer cards, with the possibility of connecting up to 20 sensors to each one.

For the generation of the experimental database a Chromalox CMXO-550 Circulating Oil Temperature Control System, designed by micro-THERMoil, (capable of heating the working fluid up to 287 °C by using up to 24 kW of power) was used as heat source. From Table 3, it can be seen that the variables measured from the hybrid GAX were the temperature at the inlet ($T_{g,in}$) and outlet ($T_{g,out}$) of the generator, the volumetric flow of the working fluid along the system's pipes (F_v), and the heat at the evaporator measured for both NH_3 (Q_{ev,NH_3}) and H_2O (Q_{ev,H_2O}). A database consisting of 3,273 elements for each of the

previously mentioned variables was obtained and used to calculate the GAX system's coefficient of performance (COP) for both NH_3/H_2O , based on:

$$COP_X = \frac{Q_{ev,X}}{Q_{gen} + W} \quad (1)$$

where X can be either NH_3 or H_2O , depending on the COP that is calculated. Normally, COP is evaluated only by considering the refrigerant used for the system; in this case, NH_3 . However, in the present work it is calculated for H_2O , which gives energy to NH_3 ; and also for NH_3 , which receives such energy and uses it through the GAX system. Theoretically, both COPs should be equal; however, by computing both coefficients and as an experimental system is being considered, it will be possible to visualize the variations in the system's performance due to

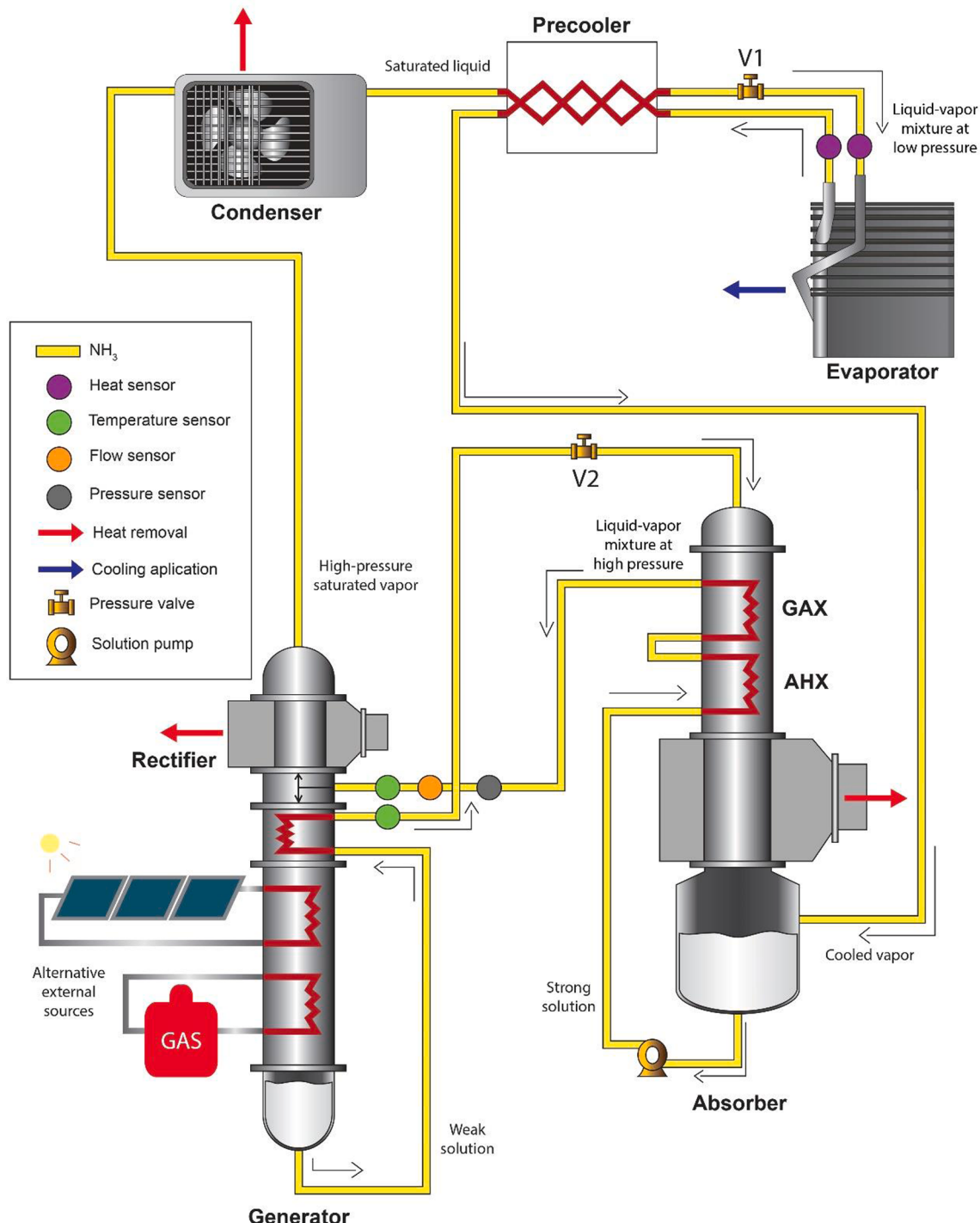


Fig. 2. Schematic diagram of the GAX cycle, integrated by a generator column with a coupled rectifier, condenser, precooler, evaporator and the absorber column with the GAX and AHX sections.

convection and radiation heat losses at the surface of each component [30,31], among other factors. As for the other elements in equation (1), $Q_{ev,X}$ is the heat measured at the evaporator for both NH_3/H_2O . W is the work done by several components of the system, often considered negligible. Q_{gen} , it is the heat measured at the generator, which is obtained as follows:

$$Q_{gen} = (F_{oil})(C_{sp})(\Delta T_{oil}) \quad (2)$$

in equation (2), F_{oil} is the mass flow of the thermal oil that circulates through the generator, C_{sp} the specific heat of such fluid, and ΔT_{oil} is the

difference of temperatures measured at the inlet and outlet of the generator.

2.1. Experimental data

In this section, the original experimental data used for the creation of artificial intelligence models is presented. Each of the plots presented in Fig. 3, from (a) to (h), represent eight experimental iterations taken place in the GAX system shown in Fig. 1. Several tests were made in order to create the database, by exploring how input variables evolves when the temperature at the generator inlet ($T_{g,in}$) is modified. The x-

Table 2

Main operating conditions for the GAX system.

Mass flow			
Weak solution	(\dot{m}_{ws})	13.302x10 ⁻³ kg/s	
Strong solution	(\dot{m}_{ss})	22.556x10 ⁻³ kg/s	
Refrigerant	(\dot{m}_{ref})	9.263x10 ⁻³ kg/s	
Cooling air at the absorber	(\dot{m}_{ab})	1.306m ³ /s	
Cooling air at the condenser	(\dot{m}_{co})	1.410m ³ /s	
Cooling air at the rectifier	(\dot{m}_{re})	0.270m ³ /s	
Heating oil	(\dot{m}_{heat})	0.122kg/s	
Ammonia concentration			
Weak solution	(NH_3_{ws})	3.99%	
Strong solution	(NH_3_{ss})	43.15%	
Refrigerant	(NH_3_{ref})	99.39%	
Cold water generation			
Input evaporator temperature	(H_2O_{in})	16 °C	
Output evaporator temperature	(H_2O_{out})	10 °C	
Mass flow	(H_2O_{flow})	0.419kg/s	
Pressure			
Generator	(P_{ge})	2.0MPa	
Condenser	(P_{co})	2.0MPa	
Evaporator	(P_{ev})	0.5MPa	
Absorber	(P_{ab})	0.5MPa	

Table 3

Design parameters obtained from the experimental system.

Variables	Symbol	Minimum	Average	Maximum	Units
<i>Inputs</i>					
Temperature at the generator inlet	$T_{g,in}$	76.5537	153.8026	188.5898	°C
Temperature at the generator outlet	$T_{g,out}$	51.8770	122.2785	147.2881	°C
Volumetric flow	F_v	13.3158	16.6071	18.9092	L/min
Heat at the evaporator for NH_3	Q_{ev,NH_3}	0.0021	5.3299	14.8104	kW
Heat at the evaporator for H_2O	Q_{ev,H_2O}	0.4235	4.1178	8.5210	kW
<i>Outputs</i>					
Coefficient of performance for NH_3	COP_{NH_3}	0.0004	0.4705	1.9725	–
Coefficient of performance for H_2O	COP_{H_2O}	0.0127	0.3532	1.6413	–

axis in Fig. 3 represents the number of samples taken every-five minutes from the experimental system. The y-axis at the left side represents the temperature scale for both inlet ($T_{g,in}$) and outlet ($T_{g,out}$) temperature measured at the generator. The first y-axis at the right side is for the heat measured at the evaporator, both for NH_3 (Q_{ev,NH_3}) and H_2O (Q_{ev,H_2O}); while the second y-axis at the right side is for the volumetric flow of the working fluid (F_v).

By analyzing each of these plots, it can be seen that for every iteration, $T_{g,in}$ is always higher than $T_{g,out}$. This indicates that the generator is using the energy received from external sources to heat the working fluid, who carries this energy along the cycle to the sections where it is demanded, and comes back to the generator with a lower amount of heat. For the discussion of the heat measured at the evaporator, it is appreciated in Fig. 3 from (a) to (c) and from (g) to (h), that Q_{ev,NH_3} presents a general tendency to be higher than Q_{ev,H_2O} , since the H_2O gives energy to NH_3 and carries it through the GAX system. However, Fig. 3 from (d) to (f), both Q_{ev,NH_3} and Q_{ev,H_2O} present similar values. This is due to the fact that the average temperature difference between $T_{g,in}$ and $T_{g,out}$ is 20 °C, which is smaller than the one presented in Fig. 8 (a) to (c) and (g) to (h), making it difficult for NH_3 to absorb heat from H_2O . As for the volumetric flow, it is a variable that shows a mirror effect when

compared to the temperatures measured at the generator; when F_v presented a growing behavior in Fig. 3 from (a) to (h), $T_{g,in}$ and $T_{g,out}$ tend to decrease. Such relations had been reported by other authors [14,15,22], mentioning that a slower flow of the working fluid implies a higher temperature at the sections where it passes, as it stays more time in them.

3. Methodology

Fig. 4 illustrates the numerical approach applied in this study, divided in three parts. In the first stage, a working database (summarized in Table 3) is created based on several tests performed on the experimental system. The numerical information is correlated to evaluate the strength of the relationship between each pair of variables. In this stage, the variables are also normalized to align them in the same range and facilitate computational models training. In the second stage, the database is divided into subsets to develop the artificial intelligence models and then their performance is compared to identify the one that best represents the thermal performance of the GAX system. Finally, in the third stage, a sensitivity study is carried out to quantify the impact of each input variable with the system's performance.

3.1. Database obtaining and analysis

The independent variables contemplated to develop the artificial intelligence models that estimate the COP of the GAX cycle where: the inlet ($T_{g,in}$) and outlet ($T_{g,out}$) temperature at the generator, volumetric flow of the working fluid (F_v), and the heat at the evaporator (Q_{ev,NH_3} , Q_{ev,H_2O}). These variables were selected due to their relevance to the system's performance coefficient for both NH_3/H_2O , which compounds the GAX cycle's working fluid [12,15]. Table 3 summarizes the information of the parameters contemplated for the development of artificial intelligence models, considering their range of operation.

Once the database was created, a correlation analysis was conducted to determine any redundant variable selection. The numerical data is then normalized in the range between zero to one, according to [32]:

$$y_N = \frac{y - y_{min}}{y_{max} - y_{min}} \quad (3)$$

where y is the set of experimental values obtained for a specific variable, y_{min} and y_{max} the minimum and maximum for such set, respectively, and y_N the normalized set of values. Normalized database was randomly divided allocating 70 % for the development of artificial intelligence models (training data), and the remaining 30 % for the cross-validation and testing processes. These percentages were selected based on accurate AI models obtained by other authors, when using such data distribution for the training, validation and testing of large datasets [33–35]. By considering these divisions, it is possible to reduce the errors associated with the model, while improving the statistical indicators used in the present study, which are described in section 3.2.4 Statistical evaluation. The experimental data used for the creation of the AI models is shown in Section 2.1.

3.2. Artificial intelligence models

In order to find a model which best represents the thermal performance of the GAX system, three artificial intelligence techniques were evaluated: Artificial Neural Networks (ANN), Support Vector Machine (SVM), and Genetic Programming (GP). Their choice was because they have reported excellent results in modeling complex thermal processes, but have different characteristics during the modeling process: ANNs are a powerful tool when having a large database with complex relationships between inputs and outputs [36]; SVM is known for its robust classification and pattern recognition ability [37]; while GP uses the concept of survival of the fittest to determine the best elements that will

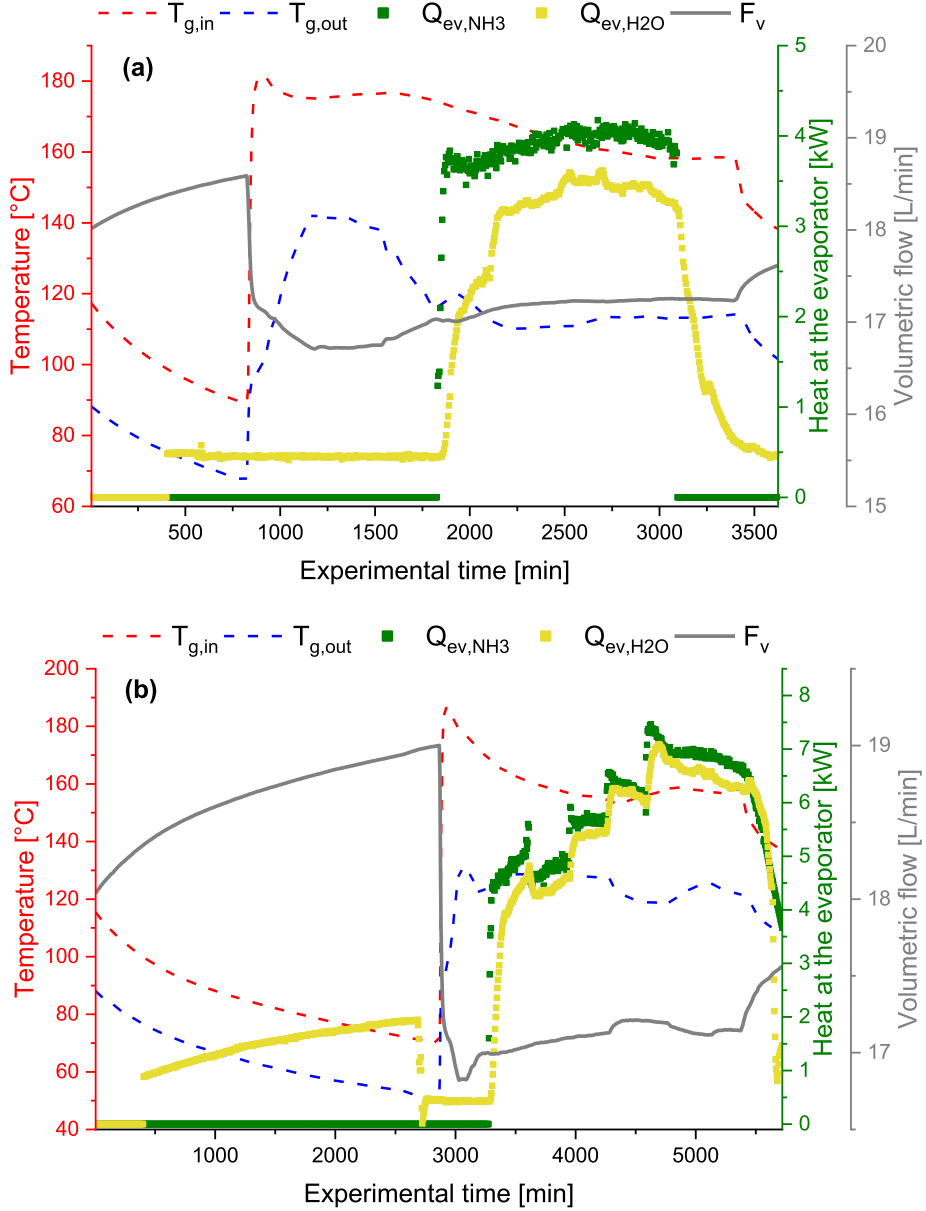


Fig. 3. Original experimental data plotted for eight iterations, (a) to (h), of the experimental GAX system.

be used in the model's creation [38]. Furthermore, these models were chosen as they have proven to be accurate, when it comes to representing different thermodynamic cycles [17,39,40]. Before using these techniques for the creation of the models, a statistical analysis will take place, in order to reduce any possible dimensionality redundancy from the studied variables. That is why other AI options, such as siamese neural networks and convolutional neural networks, were not considered for the present work, as they are useful when the complexity of the problem relies on the dimensions, classification, and preprocessing of the database [41,42].

3.2.1. Artificial Neural Network (ANN)

ANNs are a multivariate modeling technique inspired by the parallel processing of information inside the human brain. They are composed of an interconnected layer topology, illustrated in Fig. 5(a). The input layer comprises the independent variables of the problem to be analyzed. The activation potential ($n_{ANN,r}$) for a given neuron r of the ANN model can be described as:

$$n_{ANN,r} = w_{r,1}x_{ANN,1} + w_{r,2}x_{ANN,2} + \dots + w_{r,p}x_{ANN,p} + b_{ANN,r} \quad (4)$$

where p indicates the number of inputs, $w_{r,p}$ the interconnecting weight between inputs (x_{ANN}) and neurons and $b_{ANN,r}$ the bias assigned to each neuron. The activation functions, represented as f in Fig. 5(a), are in charge of receiving the activation potential and convert them into an output that will be later received by another neuron [10]. Finally, the neurons at the output layer are associated with the dependent variables of the phenomenon [43]. Considering the activation functions *Tansig* for the hidden layer and *Purelin* for the output layer, the network's result is obtained by:

$$y_{ANN} = \sum_{r=1}^R \left[w_r \left(\frac{1}{1 + \exp\left(-\left(\sum_{p=1}^P (w_{r,p}x_p) + b_{ANN,1,r}\right)\right)} \right) \right] + b_{ANN,2} \quad (5)$$

where y_{ANN} is the output generated by a neuron in the output layer, R is the total number of neurons in the hidden layer, and P the number of

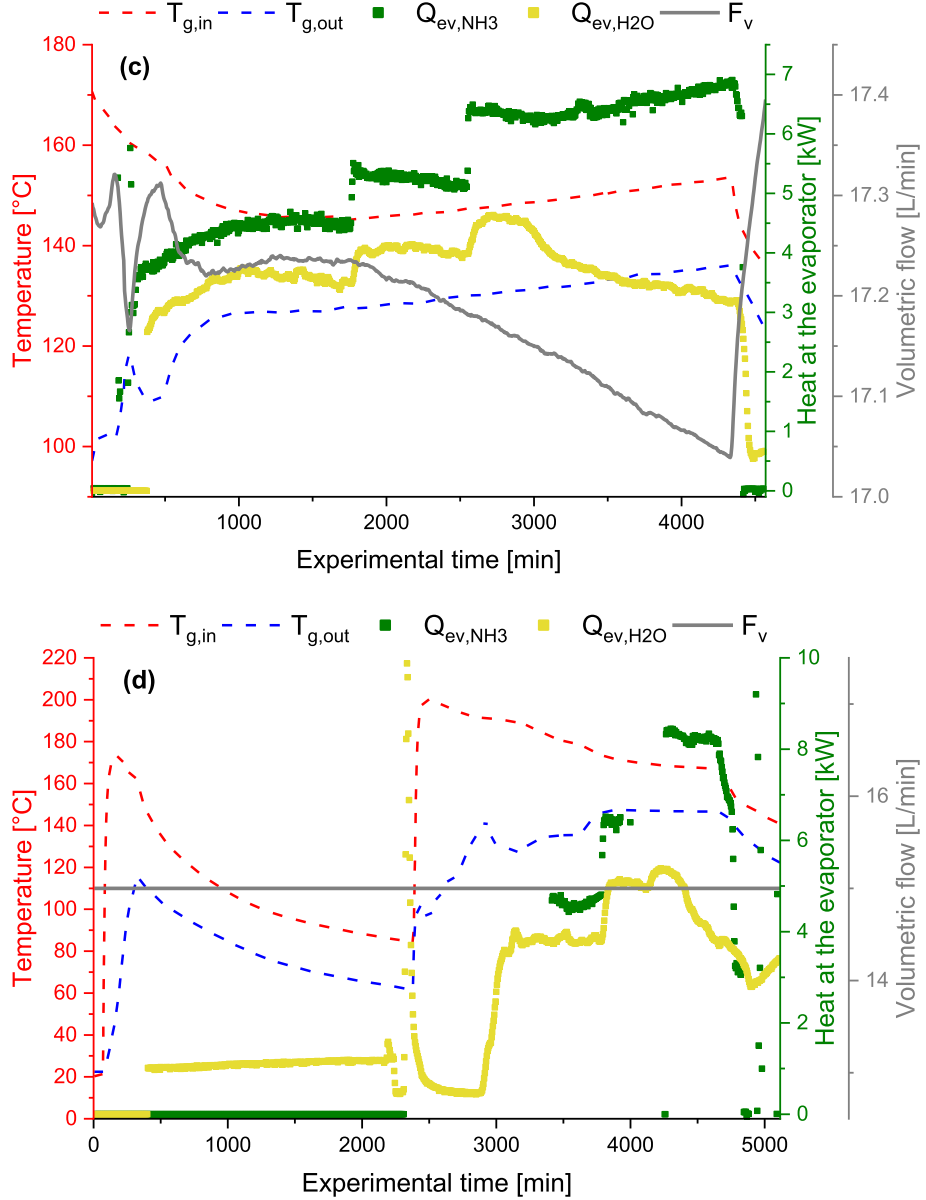


Fig. 3. (continued).

input variables. ANNs correlate the input data with the desired values by an iterative process called learning. During learning, the training data subset is used to find the values of the weight and bias matrices that best fit the desired targets in the output layer. This process is carried out through a reinforcement algorithm known as backpropagation.

3.2.2. Support Vector Machine (SVM)

As ANN can be very sensitive to the presence of noise in the database, Support Vector Machine (SVM) presents itself as a type of machine learning model, capable of solving classification problems and regression analysis [37]. This model based on the principle of structural risk minimization [44], works by changing the nonlinear input data through the kernel layer (Fig. 5(b)), to a space with properties that possess higher dimensions. Within this space, it is possible to do a nonlinear mapping in order to find a hyper-plane [45], where the relation between the output and several inputs is found. As it is a regression technique, it is capable of relating one output to multiple inputs through [46]:

$$f(x) = w^T K(x_{SVM}) + b_{SVM} \quad (6)$$

where $K(x_{SVM})$ is the space with higher-dimension properties, x_{SVM} is the input's space, w^T the weight vector and b_{SVM} the bias parameter. In Fig. 5 (b), c_m is used to represent the weight of each element in the kernel layer associated to the output of interest. The regression process considers a loss function (ϵ) in order to minimize $\|w\|^2$ and therefore reduce the model's complexity. This simplifying process takes place with the use of slack variables ($\vartheta_i, \vartheta_i^*$), which are used to measure the deviance of the samples used for training outside the intensive zone for each output i [47]. Taking these conditions in consideration, the process for the SVM regression can be stated as the minimization of the decision function J , defined as:

$$J = \frac{1}{2} \|w\|^2 + C \sum_i^n (\vartheta_i + \vartheta_i^*) \quad (7)$$

where $\|w\|^2$ is the weight Euclidian vector norm and C is the regularization constant, used as the trade-off between the model's simplicity and the error obtained by training [46]. This function is subject to the following constraints:

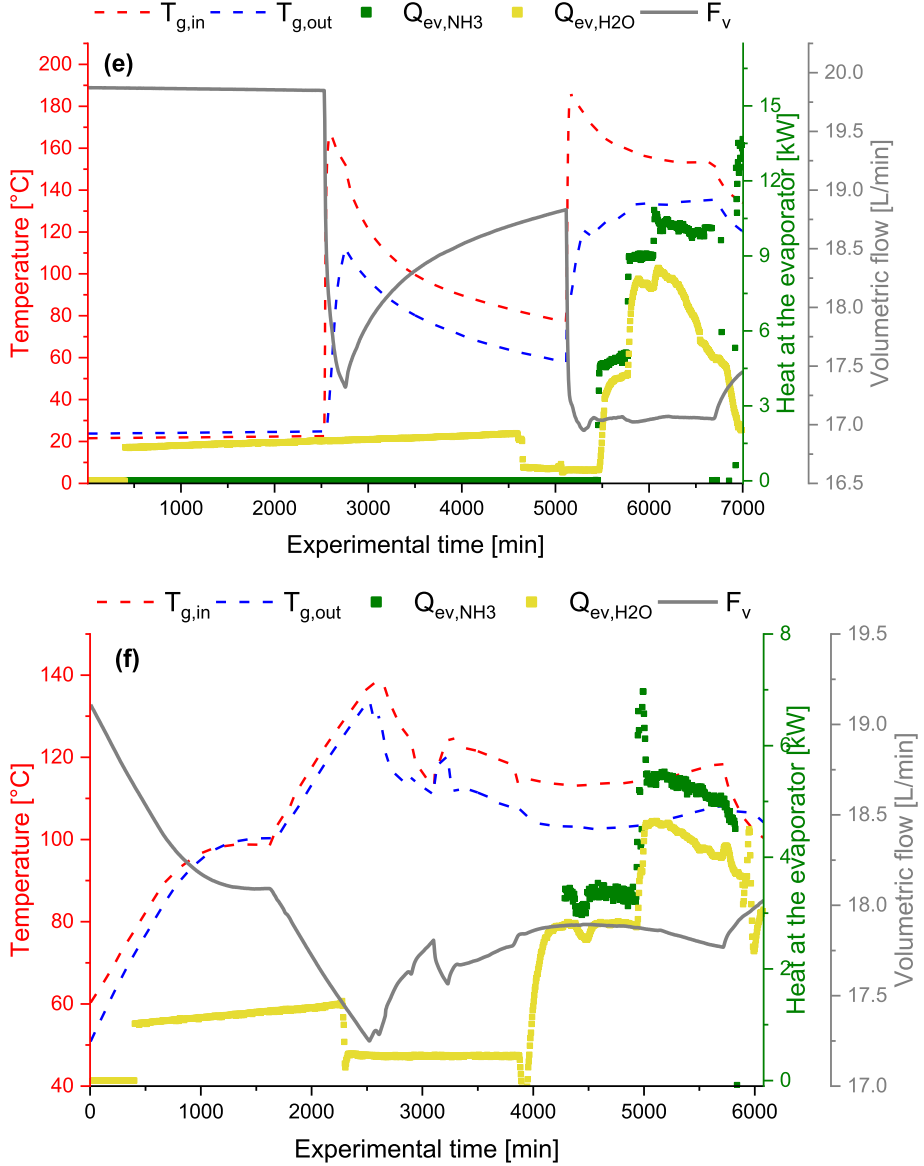


Fig. 3. (continued).

$$f(x)_i - w^T K(x_{SVM,i}) - b_{SVM} \leq \epsilon + \vartheta_i$$

$$w^T K(x_{SVM,i}) + b_{SVM} - f(x)_i \leq \epsilon + \vartheta_i^* \quad (8)$$

$$\vartheta_i, \vartheta_i^* \geq 0$$

by using the Lagrange multipliers and using the optimal constraints, equation (7) can be rewritten as:

$$y(x) = \sum_i^{n_{SVM}} (\alpha_i + \alpha_i^*) K(x_{SVM,i}, x_{SVM}) + b_{SVM} \quad (9)$$

where n_{SVM} is the number of support vectors, $K(x_i, x)$ the kernel function and α_i, α_i^* are the Lagrange multipliers, subject to $0 \leq \alpha_i, \alpha_i^* \leq C$ [48]. According to the way in which mapped inputs are distributed along the hyper-plane, it is possible to use a set of specific functions, with the purpose of finding the one that best fits the input data. The output architecture of the SVM used in the present work is:

$$y_{SVM} = \sum_i^n (\alpha_i - \alpha_i^*) \exp\left(\frac{-|x_{SVM,i} - x_{SVM}|^2}{2\sigma^2}\right) + b_{SVM} \quad (10)$$

the accuracy of the model is susceptible to the parameters σ, ϵ and C , which are cost misclassification numbers. For the present study, the set of SVM functions considered are: linear, quadratic, cubic, fine Gaussian, medium Gaussian and coarse Gaussian. Two models are created with the use of SVM, one for each of the output variables declared previously in Table 3.

3.2.3. Genetic Programming (GP)

Based on the principle of Darwinian natural selection [49], Genetic Programming (GP) consists of a process that begins with the creation of a random set of individuals, or genes, that represent the connection between independent and dependent variables (Fig. 5(c)). By evaluating the performance of this individuals to obtain the existing relations in the database, a progenitor selection takes place, in order to create a new generation. Then, an offspring generation is created by means of mutation and crossover. The performance of this new population is again evaluated, discarding the individuals with the lowest yield and inheriting the best individuals to a new generation. The cycle ends when a stopping criteria, such as number of generations or a specific performance value is achieved [50].

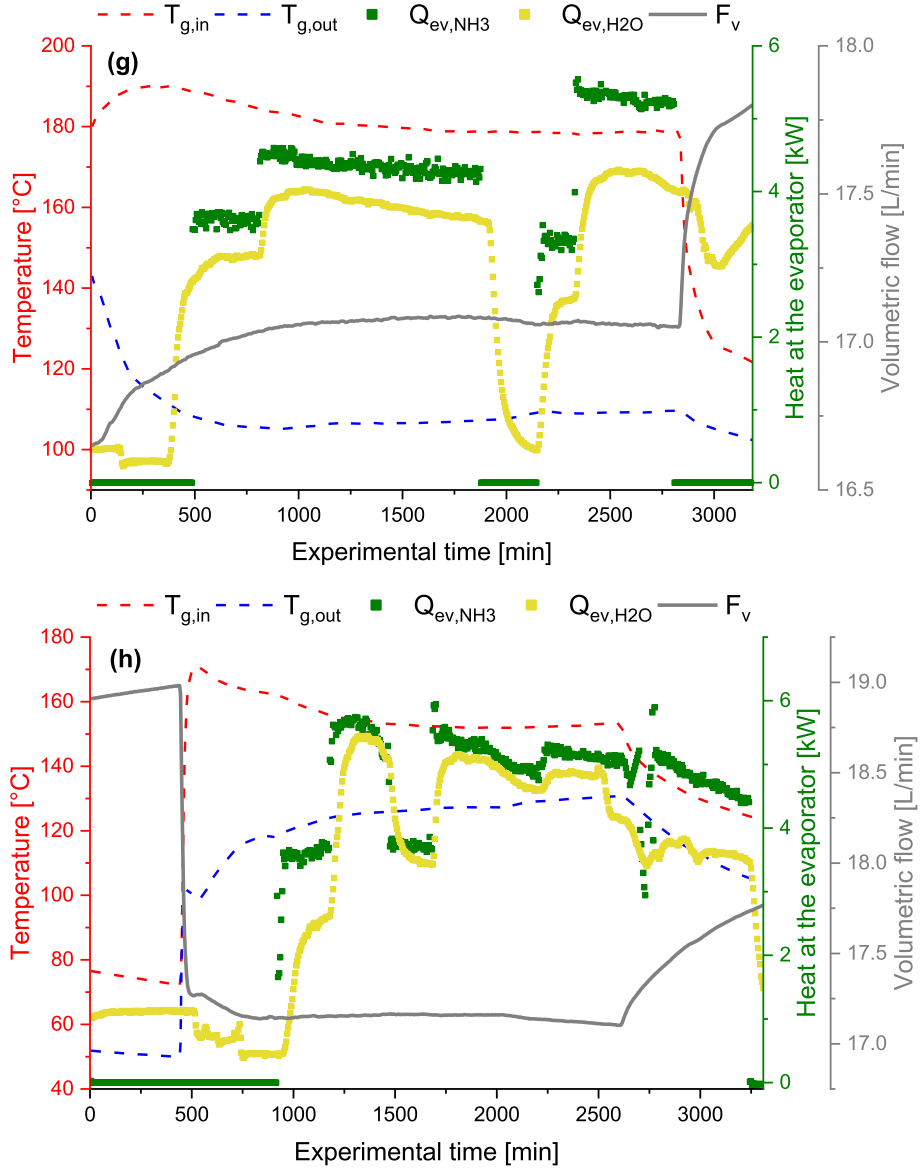


Fig. 3. (continued).

The model obtained by GP can be represented by a syntax tree, which includes the mathematical operations applied to each independent variable, in order to relate them with the desired output. Just like SVM, GP is only capable of creating a model between one output and multiple inputs. Some of the parameters that are able to be modified in order to find the best GP model are the tree depth, population, mathematical functions used to associate each gene, number of genes and generations. For the present study, the tree depth and population are fixed, while varying the number of genes and generations. The equation that describes this process is [51]:

$$y_{GP} = h_1 G_1 + h_2 G_2 + \dots + h_{n_{GP}} G_{n_{GP}} + b_{GP} \quad (11)$$

where y_{GP} is the output generated by the model, h_i is the weight associated to each gene G_i , and b_{GP} is the bias value. The subscript i considers all the n_{GP} genes obtained by the model.

3.2.4. Statistical evaluation

In order to compare the performance of the three models mentioned previously, a set of four statistical parameters is used, as they help to quantify how close the predicted models results are from the experi-

mental measured values. The parameters and their corresponding equations are the mean absolute error (MAE), mean square error (MSE), root mean square error (RMSE), and the squared R coefficient (R^2) [52]. For these equations, n_{DB} is the number of elements in the database, $y_{exp(i)}$ is the experimental output, and $y_{sim(i)}$ is the simulated output obtained by the model.

$$MAE = \frac{\sum_{i=1}^{n_{DB}} |y_{exp(i)} - y_{sim(i)}|}{n_{DB}} \quad (12)$$

$$MSE = \frac{\sum_{i=1}^{n_{DB}} (y_{exp(i)} - y_{sim(i)})^2}{n_{DB}} \quad (13)$$

$$RMSE = \sqrt{\frac{\sum_{i=1}^{n_{DB}} (y_{exp(i)} - y_{sim(i)})^2}{n_{DB}}} \quad (14)$$

$$R^2 = 1 - \frac{\sum_{i=1}^{n_{DB}} (y_{exp(i)} - y_{sim(i)})^2}{\sum_{i=1}^{n_{DB}} (y_{sim(i)} - \bar{y}_{exp})^2} \quad (15)$$

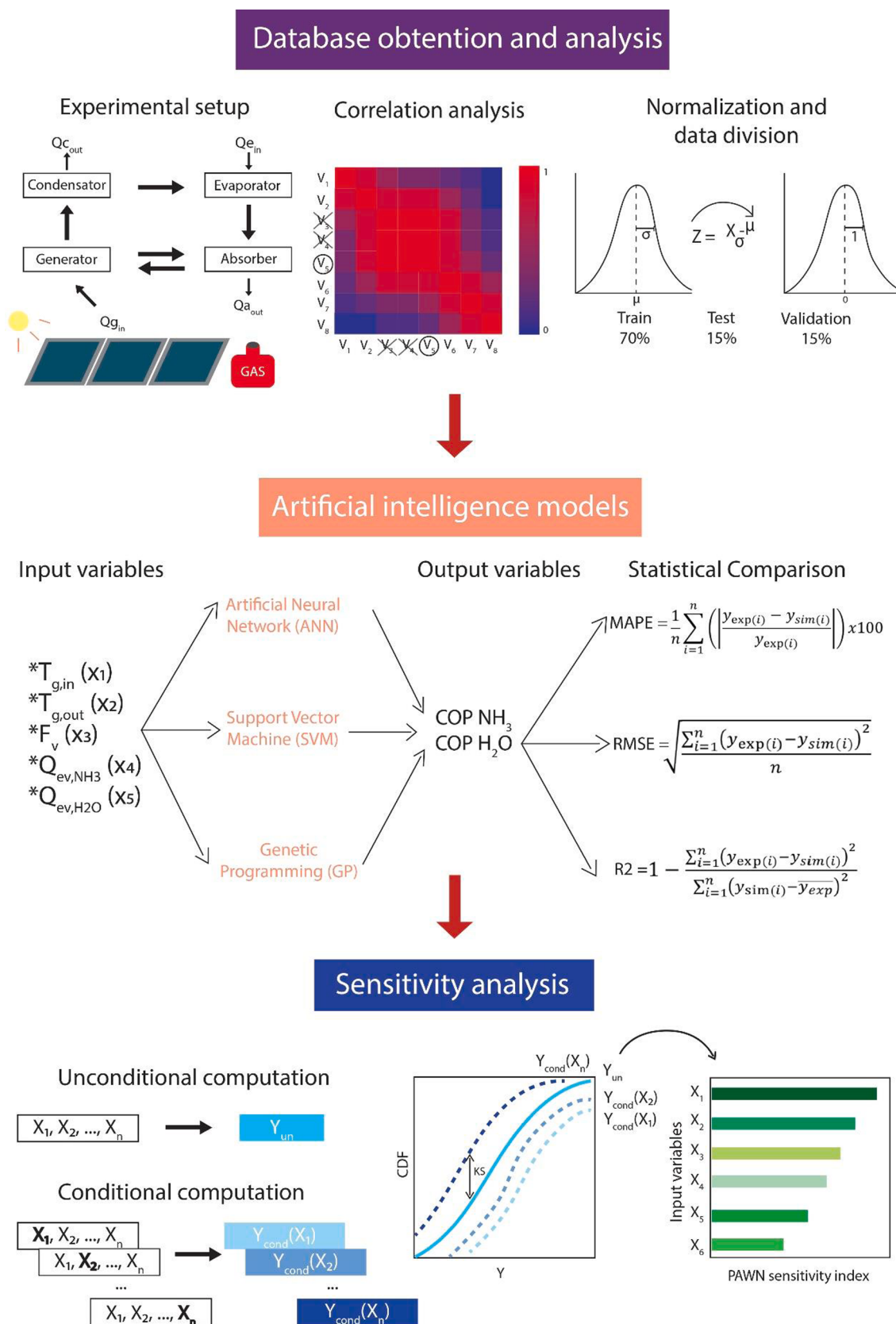


Fig. 4. Three-stage methodology procedure used to determine the impact of the design variables in the system's performance.

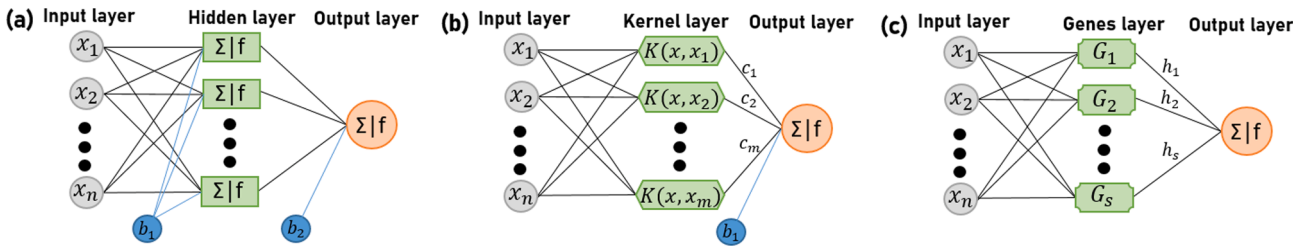


Fig. 5. Architecture of the artificial intelligence techniques used to model the GAX performance: (a) Artificial Neural Network, (b) Support Vector Machine, (c) Genetic Programming.

3.3. Sensitivity analysis

Sensitivity analysis (SA) is a technique used to determine the importance of each input variable regarding the desired output. Additionally, it is useful for interpreting the coherence of the chosen variables with the studied phenomenon. For this work, the PAWN method is chosen, as it is a powerful tool for analyzing complex computational models [53]. The method, as shown in Fig. 6, starts at phase 1 with the creation of two sets of samples, by varying all inputs simultaneously (unconditional set) and varying all inputs except for a fixed one (conditional set). For the unconditional set, \$Nu\$ random samples are generated for each input variable, and later evaluated in the computational model in order to obtain a numerical approximation of the cumulative distribution function (CDF). For the conditional sets, \$n_{SA}\$ random samples or conditioning values are created for each input variable, which are later used to approximate the CDF by considering \$Nc\$ output evaluations. For each input parameter fixed (\$\vec{X}_{1,n}, \vec{X}_{2,n}, \dots, \vec{X}_{n,n}\$), a set of CDF curves is generated at phase 2, one for each non-fixed input variable. Once all the CDF curves are created, the Kolmogorov-Smirnov statistic test (KS) is used at phase 3 to measure the distance between the unconditional CDF and the conditionals CDF. The expression used to obtain such distance is given by:

$$KS = \max_y |F_y(y) - F_{y,xi}(y)| \quad (16)$$

where \$F_y(y)\$ is the unconditional CDF, \$F_{y,xi}(y)\$ the set of conditionals CDF, and \$\max_y\$ indicates the maximum value obtained from the subtraction of both terms. Finally, considering that it exists a KS distance for every variation made in the conditional set, it is possible to compute the sensitivity index, which describes the level of relevance from each of these independent variables; the higher the index, the most important this variable is for obtaining the studied output. The equation for the sensitivity index is given by the maximum or mean KS distance [53]:

$$T_i = \frac{\text{stat}}{x_i} [KS(x_i)] \quad (17)$$

One of the main advantages from this method, taking in consideration for the study of the GAX database, is that it can be applied no matter the kind of distribution presented by the output. For the present research, it is possible to see from Section 2.1, that skewness may be presented in some independent variables, as they present a non-uniform behavior. Variance-based techniques used for the Global Sensitivity Analysis (GSA) are widely used for environmental models, as they express the relevance of each input by using their variance. However, they are not adequate for this research, as the numerical distribution presented by the input parameters may cause discrepancies when interpreting the relevance of each variable to their corresponding output. Therefore, the PAWN method is chosen to address this problem, as it is capable of efficiently computing the density-based sensitivity indices of both \$COP_{NH3}\$ and \$COP_{H2O}\$, by considering their CDF obtained with the artificial intelligence models. These functions, which are easier to derive than Probability Density Functions (PDF), are generated from the data samples of the experimental GAX system with no computing costs and

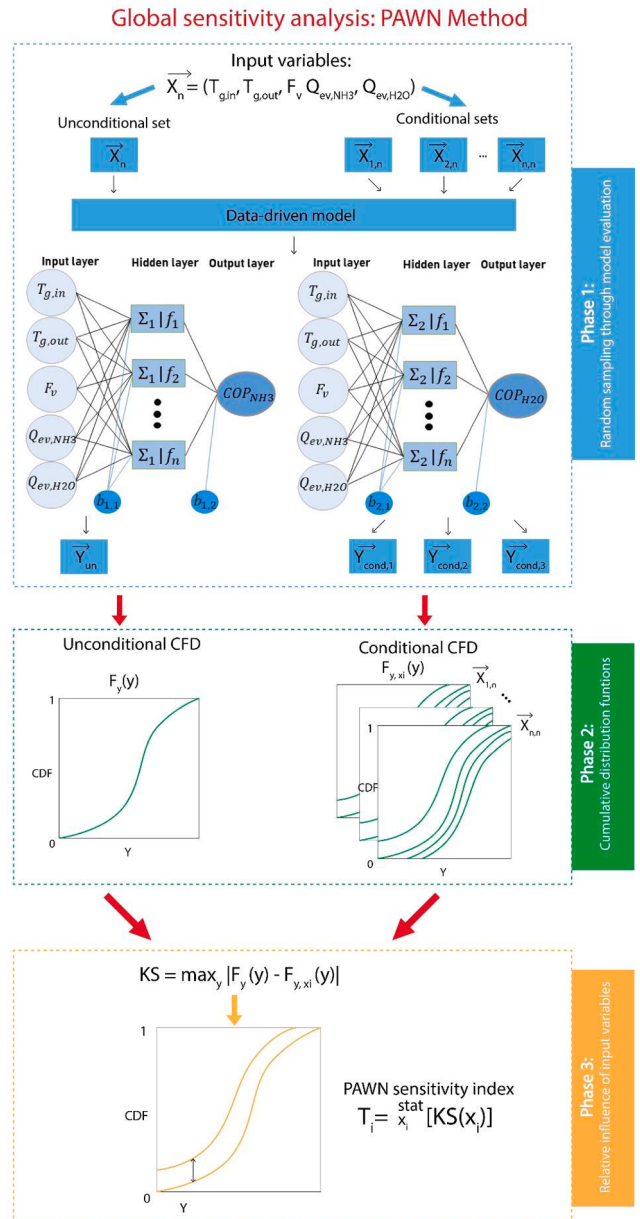


Fig. 6. Workflow of the PAWN method to determine the importance of each input parameter.

does not require any tuning parameter [54]. Additionally, this technique has been proven effectively for other refrigeration and thermal systems, where the relative influence of the independent variables with the studied outputs is investigated [55–57].

4. Results and discussion

4.1. Correlation analysis

Before using the independent variables as inputs for the creation of the artificial intelligence models, a correlation analysis was carried out for the GAX system. As it can be seen in Fig. 7, the temperature at the inlet of the generator ($T_{g,in}$) has a strong inverse correlation ($r = -0.76$) with the flow of the working fluid (F_v); this means that, when the flow slowed down, the temperature measured at the entrance of the generator tend to increased. Also, the highest direct correlation ($r = 0.66$) was the one presented between the heat measured at the evaporator for both NH_3 ($Q_{ev,NH3}$) and H_2O ($Q_{ev,H2O}$), indicating that this thermodynamic measurement presents similar results, regarding the component of the working fluid. On the other hand, the lowest correlation ($r = 0.004$) was associated to the temperature at the inlet of the generator ($T_{g,in}$) and the NH_3 heat measured at the evaporator ($Q_{ev,NH3}$), indicating that, despite both being needed for computing the COPs, such variables doesn't relate to one another.

The result obtained from the Pearson's correlation coefficient analysis indicates that each of the inputs used for the training of the models possess a unique weight that contributes to the obtaining of the COPs, which are not possible to be replaced by another independent variable measured in the present study. This fact emphasizes the need to use each of the five inputs reported for the calculation of the desired outputs.

4.2. Surrogate models of the GAX system

4.2.1. Artificial neural network (ANN)

For the ANN, different models were created by modifying the number of neurons in the hidden layer, as well as the training method used. Since the architecture starts with five input neurons, the first number of hidden neurons is selected close to such quantity, as it is one of the simplest architecture-building method [58]. However, the number of hidden neurons is considered up to 50, with the purpose of analyzing different ANN architectures along with their statistical performance. The parametric results obtained for each case are shown in Table 4. For every training method, an $R^2 > 0.98$ is always achieved. From MAE,

MSE and RMSE, magnitudes from 10^{-4} up to 10^{-13} are found immediately without the need of adding many hidden neurons. This led to choose the ANN with six hidden neurons trained with the Levenberg-Marquardt algorithm, as the artificial intelligence model obtained from this technique. Although cases with better statistical performance are presented, it is important to consider as well the computational cost required from such architectures. Therefore, the chosen ANN is capable of representing the experimental system with high precision, while reducing the computational burden associated with a high-complexity model.

4.2.2. Linear regression models

4.2.2.1. Support vector machine (SVM). Table 5 presents the statistical parameters obtained by the SVM technique, for both COP NH_3/H_2O . From the results highlighted in gray, it can be seen that Medium Gaussian is the type of SVM that best describes the experimental system, followed by the other models that work with a Gaussian kernel function. Additionally, when comparing the model's performance between ANN and SVM, there exists a notable difference in favor of ANN. The value of the parameter C used for each output was 0.1804 (COP NH_3) and 0.1292 (COP H_2O).

4.2.2.2. Genetic programming (GP). Table 6 show the statistical performance for each GP model, which were obtained by varying the number of generations from 100 up to 300 with a step of 50, and the number of genes from four to ten with a step of two. In general, both models present better results when the genetic parameters are increased. However, a considerable improvement is not perceived from any indicator when growing the generations and genes, as MAE, MSE, and RMSE remain in values from 10^{-2} up to 10^{-4} , while average R^2 presents a maximum of 0.99498 for COP_{NH_3} with 250 generations and 6 genes, and 0.99524 for COP_{H2O} with 150 generations and 8 genes.

4.3. Model validation

Once the ANN model with an architecture of 5–6–1 has been chosen as the best technique to represent the experimental data of the GAX

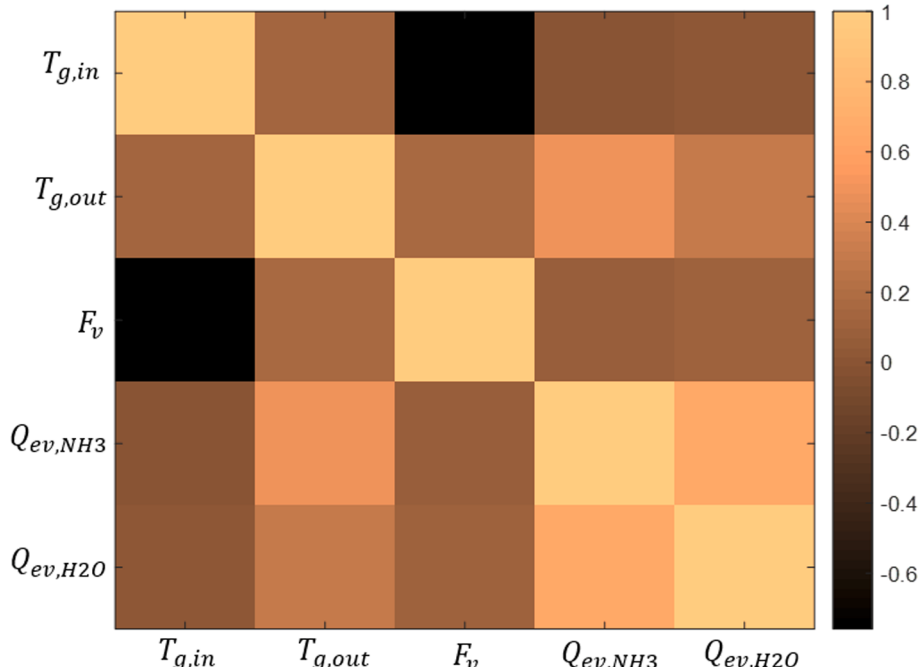


Fig. 7. Pearson's correlation coefficient obtained for the input variables of the artificial intelligence models.

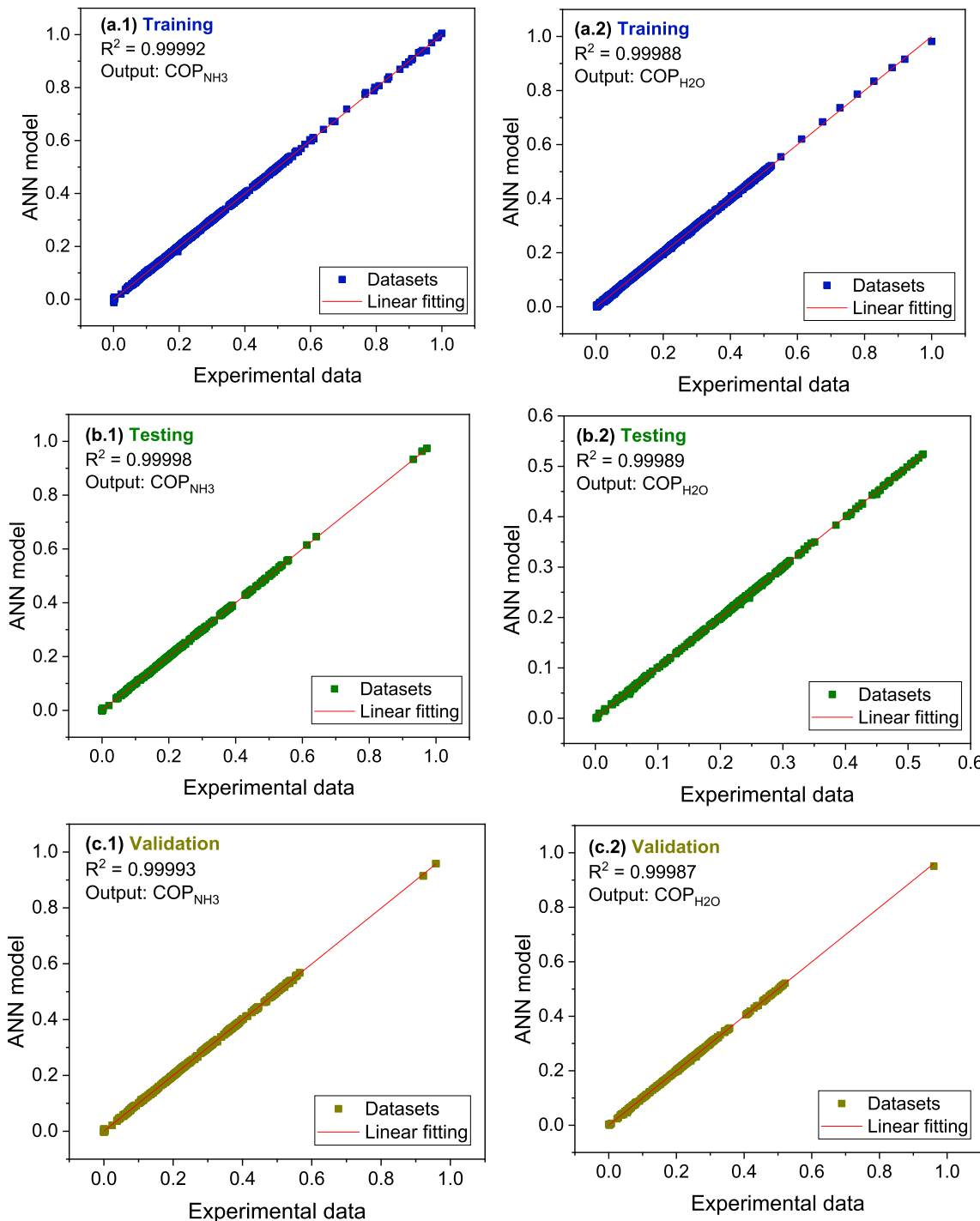


Fig. 8. Regression plots for COP_{NH_3} (a.1) Training, (b.1) Testing, and (c.1) Validation stages; and for COP_{H_2O} (a.2) Training, (b.2) Testing, and (c.2) Validation stages.

system, a validation process is taken place, in order to ensure the accuracy of the model. Fig. 8 presents the regression analysis developed for the ANN model. Fig. 8 (a.1), (b.1), and (c.1) correspond respectively to the training, testing, and validation stage of the model constructed for COP_{NH_3} . Similarly, Fig. 8 (a.2), (b.2), and (c.2) are for training, testing, and validation process of the COP_{H_2O} model. From the experimental database, 70 % of data was used for the training process, 15 % for training and 15 % for validation. As can be seen in the six regression results, by rounding the fourth decimal, an R^2 of 0.9999 or greater was always obtained for every stage. This statistical result of the linear fit for both outputs indicates that the ANN model represents, in a very precise manner, the experimental results of the GAX system.

4.4. Global sensitivity analysis

PAWN sensitivity analysis is carried out, by considering $N_u = 1,200$ as the total random samples generated for each input parameter to obtain the unconditional CDF, $N_c = 900$ output evaluations for each conditioned CDF, and $n = 70$ the number of conditioning points.

In first instance, the sensitivity index is computed for each input variable, considering their influence upon both COPs. As a preliminary visual examination of the sensitivity analysis, it is possible to determine from Fig. 9 (a) and (b) that the PAWN method converge into successful results, as the sensitivity index (T_{mn}) presents almost none or slight variations when increasing the number of model evaluations (NN). An

Table 4

Statistical performance of ANN for COP_{NH_3} and COP_{H_2O} , measured with different neural architectures and using Levenberg-Marquardt (LM), Bayesian Regulation (BR) and Scaling Conjugate Gradient Backpropagation (SCG) as training methods.

Outputs	Neural architecture of hidden layers	MAE	MSE	RMSE	R^2			Training method
					Training	Testing	Average	
COP_{NH_3}	6	8.8927x10 ⁻⁴	1.6866x10 ⁻⁷	4.1069x10 ⁻⁴	0.9999	0.9999	0.9999	LM
		0.0031	1.5164x10 ⁻⁵	0.0039	0.9984	0.9968	0.9981	BR
		0.0086	2.4053x10 ⁻⁶	0.0016	0.9873	0.9931	0.9862	SCG
	10	0.0055	0.0012	0.0345	0.9933	0.9901	0.9920	LM
		1.6539x10 ⁻⁴	8.3364x10 ⁻¹¹	9.1304x10 ⁻⁶	1.00000	1.00000	1.00000	BR
		0.0061	1.9740x10 ⁻⁵	0.0044	0.9920	0.9884	0.9919	SCG
	20	0.0030	7.6104x10 ⁻⁴	0.0276	0.9990	0.9771	0.9953	LM
		3.3261x10 ⁻⁵	8.9174x10 ⁻¹⁰	2.9862x10 ⁻⁵	1.00000	1.00000	1.00000	BR
		0.0055	1.1620x10 ⁻⁵	0.0034	0.9943	0.9963	0.9944	SCG
	30	5.2342x10 ⁻⁵	5.3923x10 ⁻⁹	7.3432x10 ⁻⁵	1.00000	1.00000	1.00000	LM
		1.0794x10 ⁻⁵	8.4473x10 ⁻¹²	2.9064x10 ⁻⁶	1.00000	1.00000	1.00000	BR
		0.0168	0.0081	0.0899	0.9665	0.9654	0.9673	SCG
	40	0.0038	0.0069	0.0832	0.9985	0.9972	0.9980	LM
		3.4215x10 ⁻⁵	2.3919x10 ⁻¹⁰	1.5466x10 ⁻⁵	1.00000	1.00000	1.00000	BR
		0.0055	5.3491x10 ⁻⁵	0.0073	0.9939	0.9967	0.9943	SCG
	50	1.5609x10 ⁻⁴	1.5485x10 ⁻⁵	0.0039	1.00000	0.9970	0.9995	LM
		1.8029x10 ⁻⁵	1.9406x10 ⁻¹¹	4.4052x10 ⁻⁶	1.00000	1.00000	1.00000	BR
		0.0085	0.0065	0.0807	0.9883	0.9853	0.9884	SCG
COP_{H_2O}	6	8.9696x10 ⁻⁴	1.0733x10 ⁻⁶	0.0010	0.9999	0.9999	0.9999	LM
		0.0052	5.7630x10 ⁻⁶	0.0024	0.9964	0.9965	0.9964	BR
		0.0070	2.0916x10 ⁻⁵	0.0046	0.9833	0.9927	0.9820	SCG
	10	0.0048	3.0161x10 ⁻⁸	1.7367x10 ⁻⁴	0.9896	0.9821	0.9882	LM
		1.8164x10 ⁻⁷	3.9009x10 ⁻⁹	6.2457x10 ⁻⁵	1.00000	1.00000	1.00000	BR
		0.0077	4.7615x10 ⁻⁶	0.0022	0.9871	0.9847	0.9877	SCG
	20	0.0029	2.2328x10 ⁻⁴	0.0149	0.9988	0.9898	0.9970	LM
		3.3825x10 ⁻⁵	5.2277x10 ⁻¹¹	7.2303x10 ⁻⁶	1.00000	1.00000	1.00000	BR
		0.0061	3.2208x10 ⁻⁵	0.0057	0.9886	0.9918	0.9890	SCG
	30	5.2942x10 ⁻⁵	4.7742x10 ⁻⁹	6.9095x10 ⁻⁵	1.00000	1.00000	1.00000	LM
		1.0984x10 ⁻⁵	2.9603x10 ⁻¹¹	5.4409x10 ⁻⁶	1.00000	1.00000	1.00000	BR
		0.0157	0.0028	0.0532	0.9515	0.9559	0.9529	SCG
	40	0.0037	0.0082	0.0908	0.9977	0.9947	0.9965	LM
		3.4702x10 ⁻⁵	4.7990x10 ⁻¹³	6.9275x10 ⁻⁷	1.00000	1.00000	1.00000	BR
		0.0050	2.5196x10 ⁻⁶	0.0016	0.9939	0.9958	0.9913	SCG
	50	1.7273x10 ⁻⁴	1.7623x10 ⁻⁵	0.0042	1.00000	0.9934	0.9989	LM
		1.6094x10 ⁻⁵	4.6064x10 ⁻¹⁰	2.1462x10 ⁻⁵	1.00000	1.00000	1.00000	BR
		0.0103	1.8709x10 ⁻⁴	0.0137	0.9749	0.9664	0.9743	SCG

increasing number of model evaluations is translated into a better convergence of the analyzed variables [59]. Also from these figures, it is seen that the inlet ($T_{g,in}$) and outlet ($T_{g,out}$) temperature at the generator are variables that significantly influence the outputs values; while the volumetric flow (F_v) almost does not seem to affect them. As for the measures made at the evaporator, Q_{ev,NH_3} has a stronger relation with COP_{NH_3} when compared with Q_{ev,H_2O} . This behavior repeats for COP_{H_2O} , where Q_{ev,H_2O} is more relevant than Q_{ev,NH_3} . When comparing these two less relevant variables for COP_{NH_3} and COP_{H_2O} , it can be seen from Fig. 9 (a) (COP_{NH_3}) that, as the number of samples (NN) increases, Q_{ev,H_2O} presents a sensitivity index greater than the one for F_v . While from Fig. 9 (b) (COP_{H_2O}), it is appreciated that Q_{ev,NH_3} and F_v presents almost the same sensitivity index for the number of samples (NN) considered. Such difference between these two Figures is explained by considering the parameters involved in equation (1). As NH_3 takes its energy from H_2O , the heat measured for H_2O at the evaporator (Q_{ev,H_2O}) is more related to an independent circuit for recirculation of H_2O located at the evaporator (in counter flow with NH_3), rather than to the volumetric flow (F_v) of the working fluid that goes through the whole cycle, for the computation of

COP_{NH_3} . On the other hand, when calculating COP_{H_2O} , the heat measured at the evaporator for NH_3 (Q_{ev,NH_3}) doesn't play such a relevant role as Q_{ev,H_2O} for COP_{NH_3} , since this heat existing in NH_3 is delivered to the different sections of the system in order for the GAX cycle to take place. Moreover, Q_{ev,NH_3} is closely related to F_v , as the adequate recirculation of the working fluid allows the ideal generation of the ammonia vapor necessary to remove the heat in the evaporator. Overall, inlet temperature at the generator appears as the variable with the most influence upon the system's performance.

Figs. 10 and 11 present the KS distances for each of the input variables, measured for COP NH_3/H_2O , respectively. The dashed red line, with a value of 0.05, represents the limit where the sensitivity stops being significant [54]. The scale of grays used to fill in the circles represents the variation in the values of the operational parameters: the lighter the circle is, the higher the value assigned to the variable.

It is possible to make a general discussion of the results based on their graphical behavior. Analyzing the temperature inlet and outlet at the generator for Figs. 10 and 11, it can be seen a similar behavior for both outputs. These variables present the strongest relation of all with their corresponding outputs, when extreme values (minimum and maximum)

Table 5Statistical performance of the Support Vector Machine (SVM) models for COP_{NH_3} and COP_{H_2O} .

Outputs	SVM models	MAE	MSE	RMSE	R^2			Kernel function
					Training	Testing	Average	
COP_{NH_3}	Linear	0.0264	0.0648	0.2545	0.9079	0.9240	0.9102	Linear
	Quadratic	0.0161	0.0024	0.0485	0.9748	0.9696	0.9741	Quadratic
	Cubic	0.0687	3.4245	1.8506	0.8326	0.8209	0.8309	Cubic
	Fine Gaussian	0.0108	0.0257	0.1604	0.9881	0.9841	0.9875	Gaussian
	Medium Gaussian	0.0109	0.0016	0.0399	0.9825	0.9911	0.9836	Gaussian
	Coarse Gaussian	0.0162	0.0057	0.0753	0.9568	0.9710	0.9590	Gaussian
COP_{H_2O}	Linear	0.0288	0.0688	0.2584	0.8070	0.8065	0.8069	Linear
	Quadratic	0.0169	0.0054	0.0738	0.9424	0.9645	0.9456	Quadratic
	Cubic	0.0659	3.2221	1.7950	0.6102	0.7752	0.6313	Cubic
	Fine Gaussian	0.0083	0.0227	0.1508	0.9900	0.9940	0.9906	Gaussian
	Medium Gaussian	0.0085	6.4055×10^{-6}	0.0025	0.9751	0.9755	0.9752	Gaussian
	Coarse Gaussian	0.0159	0.0058	0.0761	0.9233	0.9562	0.9285	Gaussian

Table 6

Statistical performance of the genetic programming models, obtained by modifying the number of generations and genes.

Outputs	Genetic variations		MAE	MSE	RMSE	R^2		
	Generations	Genes				Training	Testing	Average
COP_{NH_3}	100	4	7.813×10^{-3}	1.52×10^{-4}	1.2286×10^{-2}	0.99239	0.99469	0.99354
		6	9.78×10^{-3}	3×10^{-4}	1.701×10^{-2}	0.98584	0.98431	0.98818
		8	5.74×10^{-3}	1.3×10^{-4}	1.118×10^{-2}	0.99534	0.99435	0.99485
		10	1.142×10^{-2}	4.2×10^{-4}	2.037×10^{-2}	0.98043	0.98463	0.983
	150	4	1.734×10^{-2}	7.5×10^{-4}	2.709×10^{-2}	0.95766	0.97464	0.96917
		6	1.34×10^{-2}	8.5×10^{-4}	2.829×10^{-2}	0.98129	0.95113	0.96621
		8	1.214×10^{-2}	3.8×10^{-4}	1.905×10^{-2}	0.97516	0.98889	0.98461
		10	7.6×10^{-3}	2.9×10^{-4}	1.691×10^{-2}	0.99275	0.98669	0.98827
	200	4	8.12×10^{-3}	3.3×10^{-4}	1.808×10^{-2}	0.983	0.98781	0.98689
		6	1.096×10^{-2}	5.4×10^{-4}	2.31×10^{-2}	0.9813	0.97414	0.97854
		8	6.69×10^{-3}	1.5×10^{-4}	1.232×10^{-2}	0.99259	0.99366	0.99371
		10	8.09×10^{-3}	3.8×10^{-4}	1.906×10^{-2}	0.9905	0.97818	0.98496
	250	4	1.935×10^{-2}	1.21×10^{-3}	3.323×10^{-2}	0.96711	0.9755	0.95095
		6	5.77×10^{-3}	1.2×10^{-4}	1.098×10^{-2}	0.99514	0.99481	0.99498
		8	1.015×10^{-2}	3.9×10^{-4}	1.933×10^{-2}	0.98504	0.99192	0.98367
		10	1.068×10^{-2}	5×10^{-4}	2.198×10^{-2}	0.98393	0.98496	0.97942
	300	4	1.076×10^{-2}	5.3×10^{-4}	2.225×10^{-2}	0.98666	0.98696	0.97933
		6	8.98×10^{-3}	2.7×10^{-4}	4.631×10^{-2}	0.98969	0.988	0.98893
		8	5.92×10^{-3}	1.5×10^{-4}	1.211×10^{-2}	0.9945	0.99127	0.99378
		10	7.77×10^{-3}	1.7×10^{-4}	1.322×10^{-2}	0.9929	0.99262	0.99276
COP_{H_2O}	100	4	3.008×10^{-2}	1.88×10^{-3}	4.34×10^{-2}	0.88262	0.88212	0.87701
		6	1.227×10^{-2}	4.2×10^{-4}	2.032×10^{-2}	0.965	0.97951	0.97251
		8	6.34×10^{-3}	1.1×10^{-4}	1.031×10^{-2}	0.99227	0.99401	0.99314
		10	9.85×10^{-3}	3.1×10^{-4}	1.757×10^{-2}	0.97662	0.97657	0.97917
	150	4	2.023×10^{-2}	1.07×10^{-3}	3.269×10^{-2}	0.94146	0.92663	0.92963
		6	3.28×10^{-3}	3.3×10^{-5}	5.74×10^{-3}	0.99829	0.9975	0.9979
		8	6.17×10^{-3}	7.4×10^{-5}	8.62×10^{-3}	0.99529	0.99519	0.99524
		10	8.17×10^{-3}	3×10^{-3}	1.723×10^{-2}	0.98089	0.97747	0.98103
	200	4	5.74×10^{-3}	7.8×10^{-5}	8.82×10^{-3}	0.99457	0.99513	0.99485
		6	1.162×10^{-2}	4.2×10^{-4}	2.034×10^{-2}	0.96825	0.97147	0.97278
		8	1.101×10^{-2}	4.1×10^{-4}	1.961×10^{-2}	0.97374	0.95609	0.97269
		10	6.84×10^{-3}	2.3×10^{-4}	1.499×10^{-2}	0.98876	0.98133	0.98585
	250	4	1.104×10^{-2}	5.4×10^{-4}	2.294×10^{-2}	0.97967	0.96121	0.96524
		6	1.218×10^{-2}	5×10^{-4}	2.172×10^{-2}	0.97169	0.95163	0.96896
		8	7.44×10^{-3}	2.3×10^{-4}	1.444×10^{-2}	0.98587	0.99402	0.98642
		10	7.8×10^{-3}	2×10^{-4}	1.384×10^{-2}	0.98184	0.98709	0.987
	300	4	7.81×10^{-3}	2×10^{-4}	1.405×10^{-2}	0.9863	0.98245	0.98671
		6	6.14×10^{-3}	1.3×10^{-4}	1.102×10^{-2}	0.99388	0.99379	0.99211
		8	8.68×10^{-3}	2.7×10^{-4}	1.637×10^{-2}	0.97901	0.98325	0.9825
		10	7.24×10^{-3}	2.6×10^{-4}	1.515×10^{-2}	0.99006	0.97034	0.98452

By analyzing the statistical performance of the models obtained by ANN, SVM, and GP, the ANN is the one that best represents the experimental system. Therefore, it will be used in the global sensitivity analysis, in order to measure the influence of each input variable with respect to the COPs associated as output variables.

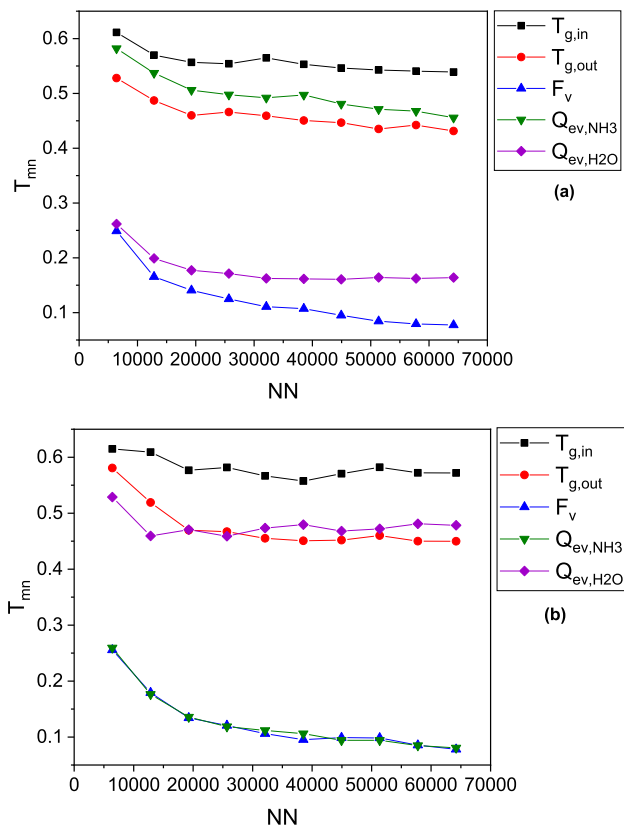


Fig. 9. Convergence analysis plots for (a) COP_{NH_3} and (b) COP_{H_2O} .

are assigned to them. While in the middle section, they almost don't relate to the output, as their KS distance are the closest possible to the dashed line. The KS distances measured for both Q_{ev,NH_3} and Q_{ev,H_2O} indicate a clear relation with their corresponding COP. As it can be seen for Q_{ev,H_2O} in Fig. 10, it almost had no impact on the output COP_{NH_3} . However, Q_{ev,NH_3} shows a strong relation with the output, mostly at low values. This same analysis can be made in reverse for Fig. 11. For such output (COP_{H_2O}), Q_{ev,NH_3} presents almost no relation with it, unlike Q_{ev,H_2O} , who presents almost the same behavior as Q_{ev,NH_3} in Fig. 10. As for the volumetric flow (F_v), this variable doesn't present a strong relation with the system's performance at any given value.

A more specific discussion is made considering the physical and thermodynamic characteristics of the system. When analyzing the KS distances obtained from each input variables, it can be seen that the greatest KS distances are for the temperature at the generator inlet ($T_{g,in}$). When assigned with the lowest numerical values (lighter circles), $T_{g,in}$ shows itself as the variable with highest influence for both COP_{NH_3} ($KS_{max} = 0.5353$, Fig. 10) and COP_{H_2O} ($KS_{max} = 0.5697$, Fig. 11). This result is in agreement with optimization studies reported in literature, which establishes that lower generator temperatures are capable of minimizing different exergoeconomic parameters [60].

For COP_{NH_3} (Fig. 10) and continuing in a descendent order regarding the maximum KS distance, the heat at the evaporator for NH_3 (Q_{ev,NH_3}) is the second variable with the highest maximum KS distance. For this parameter, it can be appreciated in Fig. 10 (c) that the maximum KS distances are achieved with the lowest numerical values assigned to the variable. Such behavior is due to the fact that the evaporator requires the lowest possible heat values, in order to fulfill its cooling application. This specific relation between the heat measured at the evaporator and the system's COP has also been developed by other authors [12]. The third variable of importance for COP_{NH_3} is the temperature at the generator outlet ($T_{g,out}$), located at Fig. 10 (b). For $T_{g,in}$, these temperature parameters are generally more relevant to the system's

performance than any other, as they dictate the range of temperature values that are present in the generator column. Such behavior has also been noticed in other thermodynamic cycles [14,22], with conditions similar to the experimental GAX cycle of the present work. The heat at the evaporator for H_2O (Q_{ev,H_2O}), reported in Fig. 10 (d), stands as the fourth variable of importance. As this fluid has a different circuit to go through at the evaporator to achieve its cooling application, it is not as important as Q_{ev,NH_3} , when calculating COP_{NH_3} . Finally, the volumetric flow (F_v) is the variable with the lowest KS values, for both COP_{NH_3} (Fig. 10 (e)) and COP_{H_2O} (Fig. 11 (e)). However, this implies that the volumetric flow of the working fluid could be modified in order to fulfill the cycle's thermodynamic requirements, such as a specific range of temperature difference between different components, and the COP will not be significantly affected. This is also mentioned by other authors [14,26], and is important specifically for the case of the GAX cycle, as a high temperature difference between the absorber and generator columns is desired.

Analyzing now the results for COP_{H_2O} (Fig. 11), the heat at the evaporator for H_2O (Q_{ev,H_2O}) is the second variable with the highest maximum KS distance. It is seen in Fig. 11 (d) that the lower numerical values are the ones with the highest KS distances. This characteristic stays the same, regardless the obtained COP. As well as for COP_{NH_3} , the third variable of importance is $T_{g,out}$, located at Fig. 11 (b). Temperatures at the generator are established as the pair of variables that presents high KS distance for both COP_{H_2O} and COP_{NH_3} . This encourages the need to study GAX systems with generators powered by different type of renewable energy technologies, in order to explore the possibility of delivering the required temperatures in a sustainable way. The fourth variable with the greater KS distance for COP_{H_2O} is the heat measured at the evaporator for NH_3 (Q_{ev,NH_3}), at Fig. 11 (c). An analog behavior compared with COP_{NH_3} , as different fluids are being considered. Finally, the volumetric flow of the working fluid (F_v) is also the variable with the lowest KS distance; however, the observation made for such variable at the previous paragraph must be taken in consideration.

In Table 7 the minimum, mean, and maximum PAWN sensitivity index is presented for each input variable, along with its relative influence percentage. For both outputs, the inlet temperature at the generator ($T_{g,in}$) is the variable with the highest relative influence with respect the others input parameters; while the volumetric flow (F_v) is the one with the lowest. For COP_{NH_3} , the second most important variable is the heat measured at the evaporator for NH_3 (Q_{ev,NH_3}), followed by the outlet temperature at the generator ($T_{g,out}$). A similar situation presents with the sensitivity index of COP_{H_2O} , where the heat measured at the evaporator for H_2O (Q_{ev,H_2O}) is the second variable of importance, just above the outlet temperature of the generator ($T_{g,out}$).

The results obtained from the PAWN global sensitivity analysis are relevant in terms of the independent variables of the system, as it was possible to determine the most influential operating parameter ($T_{g,in}$) of the GAX cycle for the calculation of the COP. The importance of this knowledge relies on the fact that, when developing a further study with the purpose of optimizing the COP, the variables considered for such process should be in terms of the different external heat sources that could supply the temperature range demanded by the generator. In this way, the optimization process will be focused on the variable with the greatest impact on the COP of the system, saving computing time by disregarding variables of little relevance, and focusing on the different parameters of the most relevant variable that can be modified. These results open up the possibility for future studies, where the optimization process of the GAX performance can be developed in terms of the temperature range that different external heat sources could supply. Furthermore, exergoeconomic indicators may be considered for a multiobjective optimization process, in order to determine the technologies that maximize the exergetic efficiency of the system while minimizing the energy cost. This hybrid computational methodology can be extended to different thermodynamic systems, in order to determine the

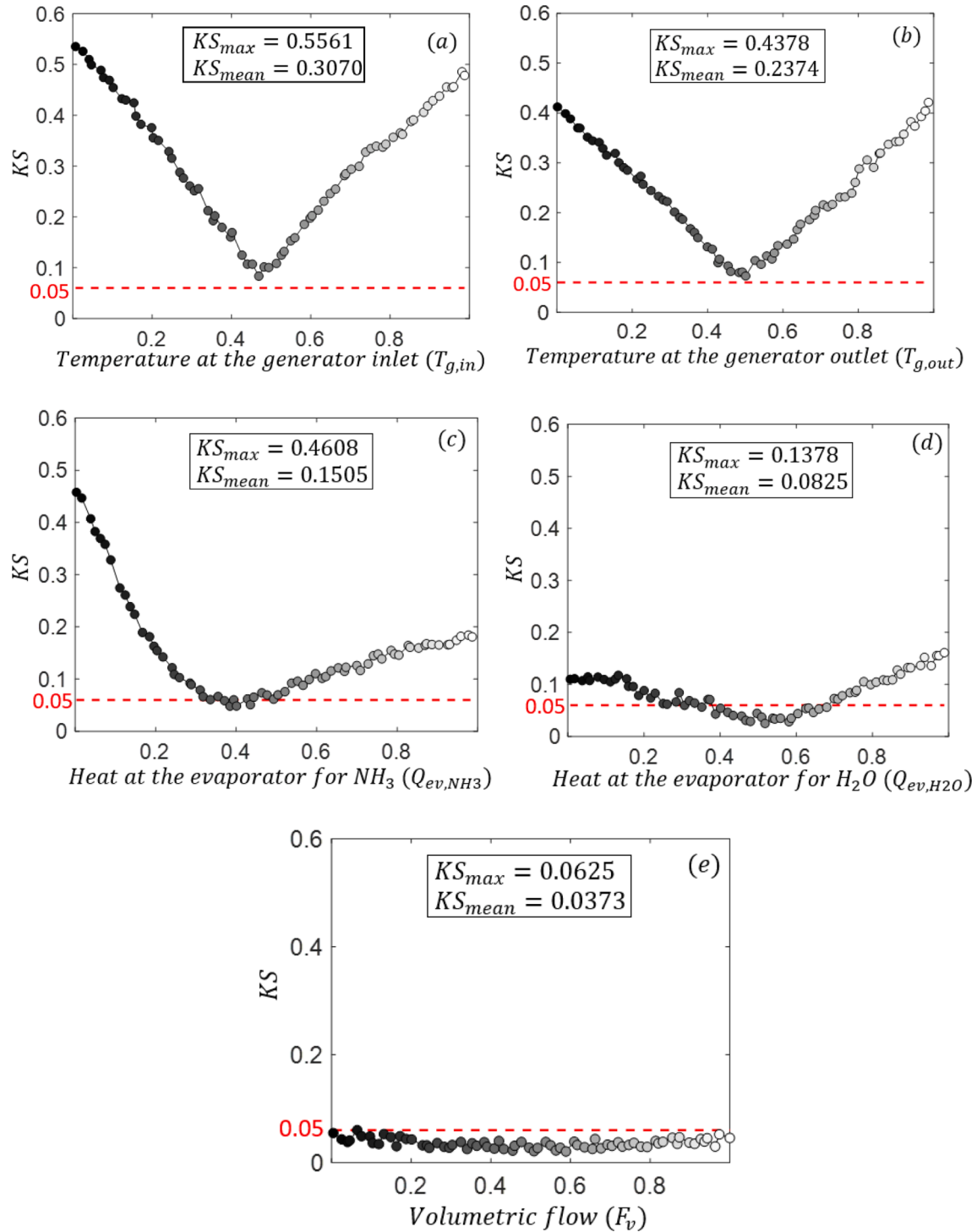


Fig. 10. KS maximum and mean distance for COP_{NH_3} measured for each input variable: (a) Temperature at the generator inlet, (b) Temperature at the generator outlet, (c) Heat at the evaporator for NH_3 , (d) Heat at the evaporator for H_2O , (e) Volumetric flow.

most relevant operating parameters in terms of a desired output, for a later simplified optimization process.

5. Conclusions and future work

In this study, a global sensitivity analysis was applied to the best prediction model of the coefficient of performance associated with a GAX experimental system, obtained from the comparison between artificial intelligence techniques ANN, SVM and GP. The input variables of such models were the operational parameters of the system: Tem-

perature inlet ($T_{g,in}$) and outlet ($T_{g,out}$) at the generator, volumetric flow of the working fluid (F_v), and the heat measured at the evaporator for NH_3 (Q_{ev,NH_3}) and H_2O ($Q_{ev,H2O}$). To compare the performance of each AI technique, the statistical indicators MAE , MSE , $RMSE$, and R^2 were used. From this work, the following conclusions were obtained:

- The best model was obtained by ANN and consists of a three-layer structure; the first layer presenting the 5 input variables, connected by the *tansig* transfer function to the second layer with 6 hidden neurons, followed by an output layer with two neurons, associated

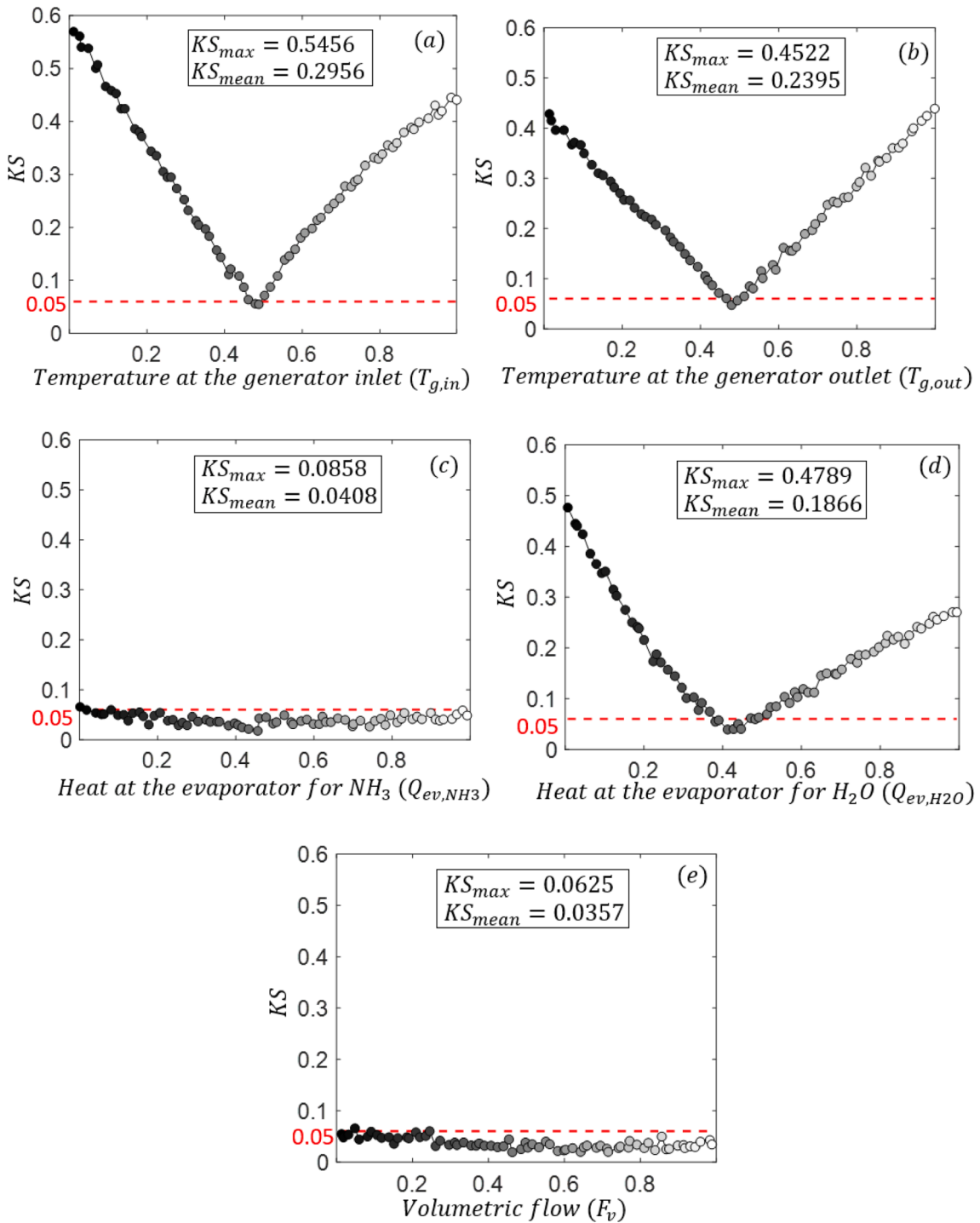


Fig. 11. KS maximum and mean distance for COP_{H_2O} measured for each input variable: (a) Temperature at the generator inlet, (b) Temperature at the generator outlet, (c) Heat at the evaporator for NH_3 , (d) Heat at the evaporator for H_2O , (e) Volumetric flow.

with the COP for both NH_3/H_2O . The model is capable of representing the experimental GAX system with a high precision, as described by the statistical performance parameters $MAE = 5.4575 \times 10^{-7}$, $MSE = 1.5278 \times 10^{-9}$, $RMSE = 2.7181 \times 10^{-5}$, and $R^2 = 0.9999$.

- A global sensitivity analysis was developed by using the PAWN method, in order to establish the importance of each input variable regarding the system's performance. The results indicate that both inlet ($T_{g,in}$) and outlet ($T_{g,out}$) temperatures at the generator where the most relevant. For the COP_{NH_3} output, the heat measured at the

evaporator for NH_3 (Q_{ev,NH_3}) was considerably more important than its analog with H_2O (Q_{ev,H_2O}). The analogous behavior occurs when analyzing COP_{H_2O} . The volumetric flow of the working fluid (F_v) was found to be the variable with less importance for both COPs.

- These results contribute to the search of better working conditions for the GAX system, as they establish the operating parameters which critically affect the coefficient of performance. In this context, it is suggested for future works to use different type of heat sources for supplying the energy required by the generator, as they are directly related with the temperatures and efficiencies measured for such

Table 7PAWN sensitivity index for COP_{NH3} and COP_{H2O}, with their relative influence percentage for each input variable.

Outputs	Input variables	Sensitivity index (T_{mn})			Relative influence percentage (%)		
		Lower	Mean	Upper	Lower	Mean	Upper
COP_{NH3}	$T_{g,in}$	0.5690	0.5578	0.6113	32.4	30.7	27.4
	$T_{g,out}$	0.4313	0.4605	0.5279	25.9	25.3	23.7
	F_v	0.0774	0.1234	0.2488	4.7	6.8	11.1
	$Q_{ev,NH3}$	0.4556	0.4987	0.5819	27.4	27.4	26.1
	$Q_{ev,H2O}$	0.1606	0.1784	0.2618	9.7	9.8	11.7
COP_{H2O}	$T_{g,in}$	0.5576	0.5803	0.6148	34.3	32.5	27.5
	$T_{g,out}$	0.4498	0.4754	0.5807	27.7	26.6	25.9
	F_v	0.0780	0.1252	0.2556	4.8	7.0	11.4
	$Q_{ev,NH3}$	0.0806	0.1262	0.2594	5.0	7.1	11.6
	$Q_{ev,H2O}$	0.4588	0.4770	0.5288	28.2	26.7	23.6

section. Additionally, it is not prolific to vary the volumetric flow of the working fluid in a wide range in order to improve the cycle's efficiency, as it is the operating parameter whose variations were less critical to such output.

- The hybridization methodology between artificial intelligence techniques and global sensitivity analysis appears as a robust and accurate approach, in order to analyze a set of independent variables measured at the experimental system. By adopting such methodology, it is possible to save computational time by disregarding variables of little relevance, and focusing on the different parameters of the most relevant variable that can be modified. Specifically, refrigeration systems along with their variables of interest may be studied through the proposed steps, for the determination of the ones that affect the most the system's output. This hybrid computational methodology can be extended to different thermodynamic systems, in order to determine the most relevant operating parameters in terms of a desired output, for a later decision making criteria based on a simplified optimization process.
- Future work aims to find the best possible configuration of the operational parameters of the GAX system, in order to obtain the highest performance possible. This objective could be approached by the use of multiobjective optimization algorithms, such as genetic algorithms, ant colony and whale optimization algorithms, where the target is to optimize the studied output by considering two or more independent variables that have an inverse relationship and are part of the calculations needed for the computation of such output. Moreover, exergoeconomic indicators may be considered for such multiobjective optimization process, in order to determine the technologies capable of supplying the heat demanded by the generator, that maximize the exergetic efficiency of the system while minimizing the energy cost.

Declaration of Competing Interest

The authors declare the following financial interests/personal relationships which may be considered as potential competing interests: Victor Cardoso Fernández reports financial support was provided by National Council on Science and Technology.

Data availability

Data will be made available on request.

Acknowledgement

The author V. Cardoso-Fernández is grateful to the financial support of CONACYT to pursue a postgraduate degree in Universidad Autónoma de Yucatán under the following quantitative details CVU: 1006703, scholarship number: 808252. The authors are grateful with Dr. Roberto Best y Brown, who led the GAX system construction and testing project,

and with the Renewable Energy Institute of UNAM, where these tests were carried out.

References

- M.E. Kahn, N. Kok, J.M. Quigley, Carbon emissions from the commercial building sector: The role of climate, quality, and incentives, *J. Public Econ.* 113 (May) (2014) 1–12, <https://doi.org/10.1016/j.jpubeco.2014.03.003>.
- A. Wang, B. Lin, Assessing CO₂ emissions in China's commercial sector: Determinants and reduction strategies, *J. Cleaner Prod.* 164 (2017) 1542–1552, <https://doi.org/10.1016/j.jclepro.2017.07.058>.
- B. Xu, B. Lin, Investigating the role of high-tech industry in reducing China's CO₂ emissions: A regional perspective, *J. Cleaner Prod.* 177 (2018) (2018) 169–177, <https://doi.org/10.1016/j.jclepro.2017.12.174>.
- J. Yang, J. Cheng, S. Huang, CO₂ emissions performance and reduction potential in China's manufacturing industry: A multi-hierarchy meta-frontier approach, *J. Cleaner Prod.* 255 (2020), 120226, <https://doi.org/10.1016/j.jclepro.2020.120226>.
- J. Evans, Technologies to Reduce Refrigeration Energy Consumption in the Food Industry, *Handbook of Waste Management and Co-Product Recovery in Food Processing* (Vol. 2), Woodhead Publishing Limited, 2009. doi:10.1533/9781845697051.2.196.
- R. Nikbakhti, X. Wang, A.K. Hussein, A. Iranmanesh, Absorption cooling systems – Review of various techniques for energy performance enhancement, *Alexandria Eng. J.* 59 (2) (2020) 707–738, <https://doi.org/10.1016/j.aej.2020.01.036>.
- R. Ahmed, S. Mahadzir, N. Erniza Mohammad Rozali, K. Biswas, F. Matovu, K. Ahmed, Artificial intelligence techniques in refrigeration system modelling and optimization: A multi-disciplinary review, *Sustainable Energy Technol. Assess.* 47 (2021) 101488.
- K.L. Cézar, A.G.A. Caldas, A.M.A. Caldas, M.C.L. Cordeiro, C.A.C. Dos Santos, K. L. Cézar, A.A.V. Ochoa, P.S.A. Michima, Development of a novel flow control system with arduino microcontroller embedded in double effect absorption chillers using the LiBr/H₂O pair, *Int. J. Refrig.* 111 (2020) 124–135, <https://doi.org/10.1016/j.ijrefrig.2019.11.014>.
- R. Alayi, A. Kasaeian, F. Atabi, Thermal analysis of parabolic trough concentration photovoltaic/thermal system for using in buildings, *Environ. Prog. Sustainable Energy* 38 (6) (2019) 13220, <https://doi.org/10.1002/ep.13220>.
- O. May Tzuc, J.J. Chan-González, I.E. Castañeda-Robles, F. Lezama-Zárraga, M. Moheno-Barrueta, M. Jiménez Torres, R. Best, Multivariate inverse artificial neural network to analyze and improve the mass transfer of ammonia in a Plate Heat Exchanger-Type Absorber with NH₃/H₂O for solar cooling applications, *Energy Explor. Exploit.* 40 (6) (2022) 1686–1711.
- M. Aprile, R. Scoccia, T. Toppi, M. Guerra, M. Motta, Modelling and experimental analysis of a GAX NH₃-H₂O gas-driven absorption heat pump, *Int. J. Refrig.* 66 (February) (2016) 145–155, <https://doi.org/10.1016/j.ijrefrig.2016.02.008>.
- M.A. Barrera, R. Best, V.H. Gómez, O. García-Valladares, N. Velázquez, J. Chan, Analysis of the performance of a GAX hybrid (Solar - LPG) absorption refrigeration system operating with temperatures from solar heating sources, *Energy Procedia* 30 (2012) 884–892, <https://doi.org/10.1016/j.egypro.2012.11.100>.
- X. Wu, S. Hu, S. Mo, Carbon footprint model for evaluating the global warming impact of food transport refrigeration systems, *J. Cleaner Prod.* 54 (2013) 115–124, <https://doi.org/10.1016/j.jclepro.2013.04.045>.
- E. Dai, M. Lin, J. Xia, Y. Dai, Experimental investigation on a GAX based absorption heat pump driven by hybrid liquefied petroleum gas and solar energy, *Sol. Energy* 169 (2018) 167–178.
- E. Dai, T. Jia, Y. Dai, Theoretical and experimental investigation on a GAX-Based NH₃-H₂O absorption heat pump driven by parabolic trough solar collector, *Sol. Energy* 197 (2020) 498–510.
- T. Jia, P. Chu, P. Dou, Y. Dai, Working domains of a novel solar-assisted GAX-based two-stage absorption-resorption heat pump with multiple internal heat recovery for space heating, *Energy Convers. Manage.* 220 (2020), 113060, <https://doi.org/10.1016/j.enconman.2020.113060>.

- [17] A. Şencan, Performance of ammonia-water refrigeration systems using artificial neural networks, *Renewable Energy* 32 (2) (2007) 314–328, <https://doi.org/10.1016/j.renene.2006.01.003>.
- [18] Y. Xu, Z. Li, H. Chen, S. Lv, Assessment and optimization of solar absorption-subcooled compression hybrid cooling system for cold storage, *Appl. Therm. Eng.* 180 (2020), 115886, <https://doi.org/10.1016/j.applthermaleng.2020.115886>.
- [19] J.U. Ahmed, R. Saidur, H.H. Masjuki, A review on exergy analysis of vapor compression refrigeration system, *Renew. Sustain. Energy Rev.* 15 (3) (2011) 1593–1600, <https://doi.org/10.1016/j.rser.2010.11.039>.
- [20] S. Anand, A. Gupta, S.K. Tyagi, Simulation studies of refrigeration cycles: A review, *Renew. Sustain. Energy Rev.* 17 (2013) 260–277, <https://doi.org/10.1016/j.rser.2012.09.021>.
- [21] M.W. Ahmad, M. Moushedi, B. Yuce, Y. Rezgui, Computational intelligence techniques for HVAC systems: A review, *Build. Simul.* 9 (4) (2016) 359–398, <https://doi.org/10.1007/s12273-016-0285-4>.
- [22] J. Wang, W. Wu, W. Shi, X. Li, B. Wang, Experimental investigation on NH₃-H₂O generator-absorber heat exchange (GAX) absorption heat pump, *Energy* 185 (2019) 337–349, <https://doi.org/10.1016/j.energy.2019.07.049>.
- [23] K.R.S. Braga Martins, J.R. Figueiredo, Computational simulation and optimization methodology of an ammonia–water GAX absorption cooling system, *J. Braz. Soc. Mech. Sci. Eng.* 41 (11) (2019) 507, <https://doi.org/10.1007/s40430-019-2004-4>.
- [24] J.R. Figueiredo, R.G. Santos, C. Favaro, A.F.S. Silva, A. Sbravati, Substitution-Newton-Raphson method applied to the modeling of a vapour compression refrigeration system using different representations of the thermodynamic properties of R-134a, *J. Brazilian Soc. Mech. Sci.* 24 (3) (2002) 158–168, <https://doi.org/10.1590/S0100-73862002000300003>.
- [25] K. Mohammadi, M. Saghafifar, J.G. McGowan, K. Powell, Thermo-economic analysis of a novel hybrid multigeneration system based on an integrated triple effect refrigeration system for production of power and refrigeration, *J. Cleaner Prod.* 238 (2019) 117912.
- [26] C. Liu, Z. Wang, W. Han, Q. Kang, M. Liu, Working domains of a hybrid absorption-compression heat pump for industrial applications, *Energy Convers. Manage.* 195 (2019) 226–235, <https://doi.org/10.1016/j.enconman.2019.05.013>.
- [27] W. Wu, M. Leung, A novel hybrid-energy heat pump with refrigerant injection: Performance characterization and injection optimization, *Energy Convers. Manage.* 208 (2020) 112584.
- [28] S.M.S. Mahmoudi, A.D. Akbari, M.A. Rosen, A novel combination of absorption heat transformer and refrigeration for cogenerating cooling and distilled water: Thermoeconomic optimization, *Renew. Energy* 194 (2022) 978–996.
- [29] N. Velázquez Limón, Estudio de sistemas de absorción avanzados para operar con gas natural asistidos por energía solar, Universidad Nacional Autónoma de México, 2002, Retrieved from https://ru.dgb.unam.mx/handle/DGB_UNAM/TES01000307973.
- [30] Y. Ai, X. Liu, Y. Huang, L. Yu, Numerical analysis of the influence of molten pool instability on the weld formation during the high speed fiber laser welding, *Int. J. Heat Mass Transf.* 160 (2020), 120103, <https://doi.org/10.1016/j.ijheatmasstransfer.2020.120103>.
- [31] Y. Ai, L. Yu, Y. Huang, X. Liu, The investigation of molten pool dynamic behaviors during the “∞” shaped oscillating laser welding of aluminum alloy, *Int. J. Therm. Sci.* 173 (2022), 107350, <https://doi.org/10.1016/j.ijthermalsci.2021.107350>.
- [32] R. Karimi, F. Yousefi, M. Ghaedi, K. Dashtian, Back propagation artificial neural network and central composite design modeling of operational parameter impact for sunset yellow and azur (II) adsorption onto MWCNT and MWNT-Pd-NPs: Isotherm and kinetic study, *Chemometr. Intell. Lab. Syst.* 159 (2016) 127–137, <https://doi.org/10.1016/j.chemolab.2016.10.012>.
- [33] Y. Xu, R. Goodacre, On Splitting Training and Validation Set: A Comparative Study of Cross-Validation, Bootstrap and Systematic Sampling for Estimating the Generalization Performance of Supervised Learning, *J. Anal. Testing* 2 (3) (2018) 249–262, <https://doi.org/10.1007/s41664-018-0068-2>.
- [34] D. Eliane Birba, D.E. Birba, A Comparative study of data splitting algorithms for machine learning model selection, Degree Project in Computer Science and Engineering, 2020, No. December.
- [35] B. Vrigazova, The Proportion for Splitting Data into Training and Test Set for the Bootstrap in Classification Problems, *Bus. Syst. Res.* 12 (1) (2021) 228–242, <https://doi.org/10.2478/busr-2021-0015>.
- [36] A. Mossalam, M. Arafa, Using artificial neural networks (ANN) in projects monitoring dashboards' formulation, *HBRJ.C.J.* 14 (3) (2018) 385–392, <https://doi.org/10.1016/j.hbrcj.2017.11.002>.
- [37] J. Cervantes, F. Garcia-Lamont, L. Rodriguez-Mazahua, A. Lopez, A comprehensive survey on support vector machine classification: Applications, challenges and trends, *Neurocomputing*, 2020, No. xxxx. doi:10.1016/j.neucom.2019.10.118.
- [38] S. Katoch, S.S. Chauhan, V. Kumar, A review on genetic algorithm: past, present, and future, *Multimed Tools Appl* 80 (5) (2021) 8091–8126.
- [39] D. Rosenberger, K. Barros, T.C. Germann, N. Lubbers, Machine learning of consistent thermodynamic models using automatic differentiation, *Phys. Rev. E* 105 (4) (2022), 045301, <https://doi.org/10.1103/PhysRevE.105.045301>.
- [40] A. Khosravi, S. Syri, X. Zhao, M.E.H. Assad, An artificial intelligence approach for thermodynamic modeling of geothermal based-organic Rankine cycle equipped with solar system, *Geothermics* 80 (2019) 138–154, <https://doi.org/10.1016/j.geothermics.2019.03.003>.
- [41] D. Chicco, Siamese Neural Networks: An Overview, 2021, 73–94, 10.1007/978-1-0716-0826-5_3.
- [42] D. Reiman, A.M. Farhat, Y. Dai, Predicting Host Phenotype Based on Gut Microbiome Using a Convolutional Neural Network Approach 2021 10.1007/978-1-0716-0826-5_12 249 266.
- [43] A.H. Elsheikh, S.W. Sharshir, M. Abd Elaziz, A.E. Kabeel, W. Guilan, Z. Haiou, Modeling of solar energy systems using artificial neural network: A comprehensive review, *Sol. Energy* 180 (January) (2019) 622–639, <https://doi.org/10.1016/j.solener.2019.01.037>.
- [44] C. Cortes, V. Vapnik, Support-vector networks, *Mach. Learn.* 20 (3) (1995) 273–297.
- [45] A. Zendehboudi, M.A. Baseer, R. Saidur, Application of support vector machine models for forecasting solar and wind energy resources: A review, *J. Cleaner Prod.* 199 (2018) 272–285, <https://doi.org/10.1016/j.jclepro.2018.07.164>.
- [46] A. Shabri Suhartono, Streamflow forecasting using least-squares support vector machines, *Hydrological Sci. J.* 57 7 2012 1275 1293 10.1080/02626667.2012.714468.
- [47] O. Kisi, J. Shiri, S. Karimi, S. Shamshirband, S. Motamedi, D. Petković, R. Hashim, A survey of water level fluctuation predicting in Urmia Lake using support vector machine with firefly algorithm, *Appl. Math. Comput.* 270 (2015) 731–743, <https://doi.org/10.1016/j.amc.2015.08.085>.
- [48] S.M. Clarke, J.H. Griebisch, T.W. Simpson, Analysis of Support Vector Regression for Approximation of Complex Engineering Analyses, *J. Mech. Des.* 127 (6) (2005) 1077–1087, <https://doi.org/10.1115/1.1897403>.
- [49] O. May Tzuc, I. Hernández-Pérez, E.V. Macias-Melo, A. Bassam, J. Xamán, B. Cruz, Multi-gene genetic programming for predicting the heat gain of flat naturally ventilated roof using data from outdoor environmental monitoring, *Meas.: J. Int. Meas. Confederation.* 138 (2019) 106–117.
- [50] J. Koza, Genetic programming as a means for programming computers by natural selection, *Statist. Comput.* 4 (2) (1994), <https://doi.org/10.1007/BF00175355>.
- [51] A.H. Gandomi, A.H. Alavi, C. Ryan, Handbook of Genetic Programming Applications, *Handbook Genetic Programming Appl.* (2015), <https://doi.org/10.1007/978-3-319-20883-1>.
- [52] O. May Tzuc, O. Rodríguez Gamboa, R. Aguilar Rosel, M. Che Poot, H. Edelman, M. Jiménez Torres, A. Bassam, Modeling of hydrothermal behavior for green facade's concrete wall exposed to nordic climate using artificial intelligence and global sensitivity analysis, *J. Build. Eng.* 33 (March) (2021) 2020, <https://doi.org/10.1016/j.jobe.2020.101625>.
- [53] E. Cruz May A. Bassam L.J. Ricalde M.A. Escalante Soberanis O. Oufram O. May Tzuc A.Y. Alanis A. Livas-García Global sensitivity analysis for a real-time electricity market forecast by a machine learning approach: A case study of Mexico International Journal of Electrical Power and Energy Systems 135 February 2021 2021 107505 10.1016/j.ijepes.2021.107505.
- [54] F. Pianosi, T. Wagener, A simple and efficient method for global sensitivity analysis based on cumulative distribution functions, *Environ. Modell. Software* 67 (2015) 1–11, <https://doi.org/10.1016/j.envsoft.2015.01.004>.
- [55] S. Chaturvedi, E. Rajasekar, Application of a probabilistic LHS-PAWN approach to assess building cooling energy demand uncertainties, *Build. Simul.* 15 (3) (2022) 373–387, <https://doi.org/10.1007/s12273-021-0815-6>.
- [56] J. Woloszyn, Global sensitivity analysis of borehole thermal energy storage efficiency for seventeen material, design and operating parameters, *Renew. Energy* 157 (2020) 545–559, <https://doi.org/10.1016/j.renene.2020.05.047>.
- [57] M. Jaxa-Rozén, A.S. Pratiwi, E. Trutnevýte, Variance-based global sensitivity analysis and beyond in life cycle assessment: an application to geothermal heating networks, *Int. J. Life Cycle Assess.* 26 (5) (2021) 1008–1026, <https://doi.org/10.1007/s11367-021-01921-1>.
- [58] K.L. Du, M.N.S. Swamy, Neural networks in a softcomputing framework, *Neural Networks Softcomputing Framework* (2006) 1–566, <https://doi.org/10.1007/1-84628-303-5>.
- [59] O. May Tzuc, A. Bassam, L.J. Ricalde, E. Cruz May, Sensitivity Analysis With Artificial Neural Networks for Operation of Photovoltaic Systems, in: *Artificial Neural Networks for Engineering Applications*, Elsevier, 2019, pp. 127–138.
- [60] T. Adibi, A.S. Mehr, Kāian-nōm o kāāz-rēgā o īkāim-iāyōdārēt īzās māyīb o Līlāt-bā. خرچ یکمیون و کاراز رگا و یکمیان یدو هر دیز اس منیب و لیل بتا. کاین نوم در این اشعا منیگ, No. September, 2020.